

## ON THE DESIGN OF SOME AIRFOILS FOR SAILPLANE APPLICATION

L.M.M. Boermans  
H.J.W. Selen  
Delft University of Technology

Presented at the XVIIth OSTIV Congress  
Paderborn, Germany  
May 1981

### INTRODUCTION

At the Delft University of Technology Low Speed Laboratory (LSL), an investigation was conducted to design and test some new airfoils for the wing of a Standard Class sailplane. To avoid building a new wing, the airfoils were designed such that just by adding material to the surface an existing wing could be modified and tested in flight. For this purpose, the ASW-19B was selected (Fig. 1) mainly because of its relatively thin wing. The manufacturer, Alexander Schleicher Segelflugzeugbau, was willing to participate in this investigation and provided two wing test segments used for wind tunnel experiments, as well as a new sailplane which was flight tested before and after the wing modification.

This paper describes the considerations, tests and results of this research. Several subjects are discussed successively:

- Wind tunnel experiments on an inner wing and an outer wing segment are described, yielding information about the quality of the actual airfoils achieved in serial production, as well as the quality of the LSL airfoil analysis and design computer program.
- The characteristics of several modern airfoils used in Standard Class sailplanes are analyzed. Typical differences in characteristics, both in cases of a smooth surface and in the case of a rough leading edge, are clarified.
- Much attention has been given to the problem of leading edge contamination by insects. Insect impact patterns, gathered in flight, show some typical airfoil related differences. Wind

tunnel measurements with real insect remains on a wing segment, and with a well known simulated bug pattern, reveal great differences in drag characteristics.

- A brief discussion is given of the application of pneumatic turbulators, a technique to reduce the drag of an airfoil rediscovered by Horstmann and Quast, DFVLR Braunschweig, and extensively tested at LSL Delft.

Based on the experience gained in these investigations, two airfoils were designed (for the inner wing and the tip of the wing, respectively) by utilizing the computer program mentioned before. The inner wing test segment was modified accordingly and tested in the LSL wind tunnel.

Next the wing of the ASW-19B sailplane was modified. Flight performance measurements were performed by DFVLR Braunschweig before and after the wing modification. Although not yet fully analyzed, the improvement is most satisfying.

### WINDTUNNEL MEASUREMENTS ON 2 SEGMENTS OF THE ASW-19B WING

At the Delft LSL, an investigation was conducted to determine the aerodynamic characteristics of two segments of the ASW-19B wing (Ref. 1). The wing design and the position of the test segments are shown in Fig. 2. The segments are situated approximately in the middle of the inner and outer wing. The inner wing segment was obtained from a wing used for static strength tests, and the outer wing segment was specially built for the present wind tunnel tests in the mold. Comparison shows that the actual airfoil shapes, measured at the segment

mid-spans, are about 1.2% chord thicker than the local design shapes (Fig. 3).

The wing segments were placed vertically in the wind tunnel test section which is 1.80 m wide and 1.25 m high. For further details, consult Ref. 1.

For accurate pressure distribution measurements the inner wing segment was provided with 107 pressure orifices (nominal diameter 0.4 mm) situated in the mid-span chord. A selection of measured pressure distributions at  $Re = 1.5 \times 10^6$  is presented in Fig. 4; Fig. 5 shows the aerodynamic characteristics. Excessive forces restricted the measurements to  $C_l < 1.5$  at  $Re = 3 \times 10^6$ .

By using a stethoscope, the oil film technique, and from pressure distributions, the following observations were made. On the lower surface a laminar separation bubble is present at all investigated Reynolds numbers and angles of attack above approximately  $-3^\circ$ . At the lower end of the low-drag bucket, when transition on the lower surface moves rapidly forward at decreasing angle of attack, no bubbles were found on the lower surface. On the upper surface the bubble is present at angles of attack up to approximately  $6^\circ$ . At higher angles of attack transition becomes the "normal" instability type (no bubble). In these cases, transition is indicated by a hump in the pressure distribution (see Fig. 4.2,  $\alpha = 8^\circ$ , 27% chord upper surface), caused by the jump in boundary layer displacement thickness and hence effective airfoil contour.

Although turbulent separation moves forward rapidly at angles of attack higher than  $10^\circ$ , the pressure distribution develops such as to cause a gradual stall.

The outer wing segment, which had no aileron, was investigated only with respect to flow behaviour and drag characteristics. Calculation showed that due to the taper ratio the greater part of the outer wing has an airfoil more resembling the inner wing airfoil than the tip airfoil. Consequently, the test results of the outer wing segment were similar to the inner wing segment results, so there was no need to provide the outer wing segment with pressure orifices. As an example, Fig. 6 shows

oil-flow patterns, made at a practical situation, where there is the "normal" instability type transition and some trailing edge separation on the upper surface, and a relatively long laminar separation bubble (11% local chord) on the lower surface.

The characteristics of the actual inner wing airfoil, named FX61-163/ASW-19B, and of the design airfoil FX61-163, were calculated with the LSL airfoil analysis and design computer program as it was available at the time the measurements took place. The results, presented in Ref. 1, indicated a slightly higher drag coefficient for the actual airfoil, while the lift versus angle of attack curves coincided. However, there was a striking discrepancy between the calculated and the measured lift versus angle of attack curve in that the measured lift was about  $C_l = 0.15$  lower than the calculated lift. This clearly demonstrated the importance of taking into account the effect of the curvature of the wake (which acts as a fluid flap). A description of the procedure, which has been incorporated in the computer program, is given in Ref. 2.

It is clear that the computer program - although not perfect in every detail as will be shown (so that wind tunnel measurements remained necessary for verification) - was an indispensable tool in the design process which ultimately led to the improved airfoils.

#### ANALYSIS OF SOME AIRFOIL CHARACTERISTICS

A comparison of the characteristics of the airfoils which are commonly used in modern Standard Class high performance sailplanes, supplemented with some calculated results, clarify some typical features.

In general, the Wortmann airfoils designed after 1964 (as FX S02-196 and FX 66-S-196V1) have lower drag coefficients at high lift coefficients than earlier designs (as FX 61-163 and FX 61-184), as shown by the examples in Fig. 7, taken from Ref. 3.

The pressure distribution of the later types is such that, in the low drag range of lift coefficients, transition

on both sides of the airfoil stays near a particular chord position. The upper end of the low drag bucket is pronounced and coincides with the maximum lift coefficient: i.e., when transition moves forward suddenly due to the development of a pressure peak on the airfoil nose, separation of the turbulent boundary layer at the rear of the airfoil follows.

On the earlier designs, the pressure distribution develops such that transition on the upper surface moves steadily in a forward direction at increasing angle of attack, thus increasing the drag (and decreasing the lift curve slope). When transition approaches the airfoil nose, the turbulent boundary layer starts to separate at the trailing edge.

On the well-known Eppler airfoil E603, transition and turbulent separation move forward steadily at the high angles of attack (instead of suddenly as on the "after 1964" Wortmann airfoils), thus rounding off just the upper edge of the low drag bucket.

In order to get some qualitative information about the effects of a rough leading edge, the characteristics of the airfoils previously mentioned were calculated at practical combinations of lift coefficient and Reynolds number, with the assumption of a turbulent boundary layer from  $5^\circ$  chord on both sides of the airfoil.

In addition to an almost doubling of the upper and lower surface drag contributions at attached flow conditions, the calculations indicated serious separation problems for the upper surface flow of the E603 and "after 1964" Wortmann airfoils, and no such problems for the earlier Wortmann designs. In the newer types, the turbulent boundary layer is not able to overcome the pressure gradients on the rear part of the airfoil up to the trailing edge.

Wind tunnel experience at LSL with roughness on the nose of FX 66-S-196V1 (as already noticed in Ref. 4) and E603 [used in the present research program (Ref. 2)], as well as the results presented in the next chapter, confirmed these predictions.

## LEADING EDGE CONTAMINATION BY INSECTS

The serious degradation of performance (increased sink rate, increased stalling speed and sometimes bad stalling behaviour) caused by insect contamination of the wing leading edge or by rain, is well-known. In order to investigate whether measures could be taken to alleviate these problems by proper airfoil design, some flight experiments and wind tunnel tests were carried out. The main results of this research, which is still going on, will be described.

In order to establish whether there is a relation between airfoil shape and insect impact pattern, as suggested in Ref. 5, flights were carried out with seven different sailplanes flying simultaneously most of the time and gathering insects on sheets of self-adhesive matted polyester film attached to the wings. The 0.08 mm thick and 0.59 m wide sheets were placed both on the left and right inner wing at equal distance from the wing root, covering about the front half of the local wing chord. After the tests, the sheets were carefully removed and pinned on frames for transport and further examination. Due to the mat coating the traces of ruptured insects could easily be found.

All sailplanes were winch-launched at Venlo (The Netherlands), sometimes more than once, and their pilots were asked to perform a normal local flight. Weather circumstances were normal for a sunny day in July and small cumulus clouds aided in thermal finding; the mean value of the reported climb rates was about 1.5 m/s. Fortunately, the density of the aerial insect population, which consisted almost exclusively of Aphids, was high; more than 3000 insects were captured. The long wet period preceding the test day many have contributed to this.

Two additional sheets to be used for the wind tunnel measurements were placed on the left and right wing of an ASW-19B, at a spanwise position corresponding to the position of the local wing chord. To simulate the surface condition of the clean wing, these sheets were painted accordingly. Nevertheless, while no difference could

be observed between the differently coated sheets, the sheets in general seemed to be slightly less contaminated than the wing surfaces adjacent. (Probably the sheets were smoother than the wing surfaces).

Since the Aphid is probably the best representative of the great majority of insects, which consist of small and relatively fragile kinds and therefore most liable to cause insect roughness, the present results may represent a severe case of insect contamination.

Table 1 lists data and main results of the insect impact measurements. The results for the left and right wing sheets were put together because they did not show any peculiar difference. Fig. 8 shows the extent of the impacts of the upper and lower surface of the local airfoil shapes. The reason for comparing the fractional chord extent of the impacts is, as elucidated in the Appendix, that this ratio depends (theoretically) on airfoil shape and speed and angle of attack, but not on the absolute size of the airfoil (i.e., chord length). Fig. 9 shows some typical insect impact distributions.

The different relations between speed and angle of attack for the non-flapped and flapped airfoils (the range of angles of attack for the flapped airfoils is much smaller) as well as the sharp nosed rather flat lower surface of the flapped airfoils, cause the great difference in insect impact distribution and extent (Table 1 and Figs. 8 and 9).

With respect to the KA-6CR results, it should be mentioned that the pilot, for reasons of staying aloft, never exceeded 110 km/h. Probably the low flight speed affected the impact pattern (fewer ruptured insects, shorter impact extent).

No correlation between airfoil thickness and the number of impacts per minute could be established. According to theory, Ref. 6, the insects are only slightly deviated by the induced velocity field set up by the airfoil; hence, less impacts could have been expected on the thinner airfoil. Although not all the results of these naturally roughened sheets can be fully explained, it is clear that there is a great difference between impact patterns of flapped and non-flapped airfoils.

While on non-flapped airfoils some 55% of the total number of impacts is found on the upper surface and 45% on the lower surface, these figures read roughly 80% and 20% for the flapped airfoil. Apart from the corresponding great difference in the fractional chord extent of the impacts, there is a trend toward a less extended impact pattern for the thinner airfoil.

However, wind tunnel measurements revealed that these results, with respect to overall leading edge contamination, are not crucial.

The thickest insect splatters, which are found on the leading edge, cause premature transition, while the remains and traces more rearward do not add any contribution to the drag. Comparison of the impact distributions in front of 1% chord and 2.5% chord, Table 1, shows that for the modern sailplanes (KA-6CR excluded) the relative differences in impact distribution on upper and lower surface (flapped and non-flapped) are quite small. Consequently, it was concluded that improvements in airfoil characteristics will have to come from proper development of the turbulent boundary layer, with at least no separation problems as on the modern airfoils mentioned before.

Wind tunnel measurements were performed with the two naturally roughened sheets attached to the inner wing test segment. The lift coefficient was found from the tunnel wall pressures and the correlation between tunnel wall pressures and lift coefficient of the clean wing. Mean drag coefficients were obtained from measured drag distributions along 0.15 m span (staying out of the turbulent wedges which occasionally originated from the rims of the sheets). The onset of turbulent flow was detected by a stethoscope.

In a similar way, the aerodynamic characteristics of the inner wing section, now provided with an artificial "bug pattern", were determined. This bug pattern, consisting of rows of little squares of silver duct tape on the leading edge of the wing, is used in the USA in measuring the performance of gliders, in an attempt to simulate a fairly severe collection of insects, Ref. 7. The simulated insects, 0.33 mm

thick and measuring 5 mm on the sides, were placed every 150 mm on the leading edge, another row in between 25 mm above the leading edge, and a third row in between and 13 mm below the leading edge.

Fig. 10 presents the results for practical combinations of angle of attack and Reynolds number.

While at lift coefficients higher than 0.8, which corresponds to speeds lower than 91 km/h at a wing loading of 32 kgf/m<sup>2</sup>, the drag curves of the artificial and real insects coincide. There is a remarkable difference at lower lift coefficients, i.e., the greater part of the speed polar where the contribution of the profile drag to the total drag of the sailplane increases with speed.

At negative angle of attack, the drag increase due to the real insects is roughly half the increase due to the simulated insects.

With respect to the real insect measurements, the stethoscope revealed that at positive angles of attack the upper surface flow was disturbed by the insects on the airfoil nose (and at angles of attack beyond 6° the area washed by turbulent flow rapidly increased) while the lower surface flow was not disturbed since the location of transition corresponded to the clean airfoil case. At negative angles of attack, it was the reverse; the lower surface flow was disturbed by the insects on the airfoil nose and the upper surface flow showed a position of transition corresponding to the clean airfoil case. At zero angle of attack, the height of the insect remains is below the critical roughness height and no drag increase results.

The left wing sheet was examined in more detail at a Reynolds number of  $1.5 \times 10^6$ . As shown in Fig. 11, the range of angles of attack is increased where the insect remains were not, or to a less extent, disturbing the flow. Also shown is the decrease of the lift curve slope and maximum lift coefficient due to the growth of the upper surface boundary layer thickness which reduces the effective camber. (Although the method to obtain the lift coefficient from wall pressure measurements is not

accurate at high angles of attack, Fig. 11, the effect of the roughened leading edge is obvious.)

Removal of the remains behind 2.5% c and 1% c, respectively, did not yield any change in characteristics at this Reynolds number. With all the insects removed, the characteristics correspond to the results obtained earlier for the airfoil without sheet.

No stethoscope measurements were performed for the artificial roughness case. However, the drag measurements show that the bugs are located such that there is no situation where none of them disturbs the flow. Moreover, the drag depends very much on the bug pattern (Ref. 1). More research is clearly necessary to determine the conditions on the airfoil nose relevant for the insect contamination case and useful for theoretical and experimental work.

#### DRAG REDUCTION BY PNEUMATIC TURBULATORS

At the Delft Low Speed Laboratory an airfoil, HQ 17/14.38 (designed by Horstmann and Quast, DFVLR Braunschweig), was extensively tested. This airfoil is being used for the ASW-22 wing, a new Open Class sailplane (24 m span) being built at Schleicher's factory now. A special feature of this airfoil is the application of pneumatic turbulators; a more detailed discussion of this subject is given in Ref. 8.

It is well known that laminar separation bubbles may spoil the initial conditions of the turbulent boundary layer, thus increasing the drag of an airfoil. Wortmann provided a solution to the problem by using a so-called instability region, a region with a slightly adverse pressure gradient which destabilizes the laminar boundary layer without causing separation (Ref. 9). Considering the various combinations of angle of attack and Reynolds number at which the airfoil should have the lowest possible drag, it is obvious that this region must be carefully designed.

Another method to decrease drag by avoiding laminar separation bubbles is to disturb the boundary layer in the vicinity of the laminar separation point by blowing air through small orifices periodically spaced in spanwise

direction. In this way, Pfenninger obtained a drag reduction for a particular airfoil at a constant angle of attack which started at  $Re = 2 \times 10^6$  and gradually increased with decreasing Reynolds number up to 40% at  $Re = 0.33 \times 10^6$  (Ref. 10).

Fig. 12 shows the drag reduction obtained by using such pneumatic turbulators on the lower surface of the HQ 17/14.38 airfoil. Although the pronounced laminar separation bubble is not completely removed in this case, the drag reduction is still up to 10%.

Also shown is the result of the LSL airfoil analysis and design computer program, showing fair agreement with the measurements except for the prediction of drag increase due to laminar separation bubbles. (Meanwhile, it has been established that the method to calculate the change in boundary layer characteristics between transition and reattachment has to be improved. Experimental research has been started.)

#### AIRFOIL DESIGN AND TEST RESULTS

Based on the experience gained in previous studies, two airfoils were designed for the inner section and tip of the ASW-19B wing. For weight reasons, the new airfoils had to fit as tightly as possible around the existing ones, especially at the aileron (flutter). This, of course, limits the designs. During the design process the effect of calculated changes in airfoil characteristics on the sailplane performance were repeatedly evaluated using the computer program for parametric sailplane performance optimization (Ref. 11).

First, the inner wing airfoil was designed. Figure 13 shows the new design, DU 80-176, fitted to the inner wing test segment airfoil. Figure 14 compares some potential flow pressure distributions and Figure 15 shows the calculated characteristics at practical combinations of lift coefficient and Reynolds number.

The upper surface was designed for a longer laminar flow extent in the case of a clean airfoil, and no separation problems with a roughened leading edge. In combination with the lower surface, the maximum lift coefficient should be

slightly increased.

The lower end of the low drag bucket was determined at  $C_l = 0.2$ , considering the sailplane penetration speeds in relation to practical climb speeds, and a margin for vertical air velocity fluctuations during the penetration phase.

Increasing laminar flow region on the lower surface, while maintaining lift (aft-loading), introduced the danger of pronounced laminar separation bubbles. Here, the use of pneumatic turbulators seemed to be promising. While fixing the position of laminar separation needed for the application of these turbulators was easy through a proper design of the pressure distribution, the desired development of the boundary layer in front of the laminar separation point needed more iterations.

According to stability theory, small harmonic disturbances in the laminar boundary layer become unstable and amplify; the amplification ratio is expressed by  $\frac{a}{a_0} = e^{\sigma_a}$ . As soon as they have gained sufficient amplification, transition occurs. However, the corresponding amplification factor,  $\sigma_a = \sigma_{\text{turb}}$ , is a function of the free-stream turbulence and other disturbances such as sound.

Consequently, different values of  $\sigma_{\text{turb}}$  (and hence different aerodynamic characteristics, in particular drag coefficients) may be valid for a given wind tunnel facility and for free flight. A detailed discussion about this phenomenon is given in Ref. 1.

The pressure distribution on the lower surface of DU 80-176 was designed such that, in situations near the lower end of the low drag bucket, the amplification factor gradually increases in chordwise direction. The effect is twofold. Due to the controlled movement of the position of transition, the drag increases more or less gradually, not suddenly as calculations indicated for the actual inner wing airfoil (Fig. 15). Secondly, in free flight conditions where  $\sigma_{\text{turb}}$  is higher than in the wind tunnel situation, the transition position starts to move forward at a lower angle of attack than in the wind tunnel, thus extending the low drag range at the lower end.

For DU 80-176, this extension would correspond to about 25 km/h in flight speed.

(It is believed that this effect causes the discrepancy which is often found when measured speed polars - in particular those of sailplanes with flaps - are analyzed by using airfoil data obtained in a wind tunnel.)

Finally, it was realized that the lower surface, squeezed out for laminar flow conditions, is not optimal in the case of a roughened leading edge. Experience will determine if maintaining adequate climbing performance will compensate for this drawback.

The inner wing test segment was modified to the new airfoil shape and the wind tunnel tests were repeated. Again, the lift coefficient was obtained from the tunnel wall pressures. The results, shown in Fig. 16 as well as in the oil-flow patterns, indicated the existence of pronounced laminar separation bubbles on the lower surface except in situations near the lower end of the low drag bucket at  $Re = 3 \times 10^6$ .

At practical combinations of angle of attack and Reynolds number, no bubble was present on the upper surface. The intended lift coefficient at the lower end of the low drag bucket and gradual drag increase below it, as well as a slightly higher maximum lift coefficient (formerly 1.39 - now 1.45), were realized.

Next, tests were performed at four practical combinations of lift coefficient and Reynolds number to determine the best location of the pneumatic turbulators, as well as the air volume flow needed to obtain the lowest drag. Forty pneumatic turbulators, consisting of 20 mm long tubes with 0.6 mm inner diameter installed with 16 mm interspace, were tested at 63, 64, 65 and 67% chord positions. (From oil-flow patterns, the laminar separation position was detected at 63-64% chord.) By pressurizing the wing test segment, the air volume flow was varied from zero up to 150  $cm^3/sec$ . While the results of the 63, 64 and 65% chord positions did not differ much (the 65% chord position showed the smoothest drag curve), the 67% chord position was clearly too far

rearward. The air volume flow needed to obtain the lowest drag was not critical; the curves showed a flat optimum. A value of 80  $cm^3/sec$  was suitable at the four practical combinations of lift coefficient and Reynolds number.

Fig. 17 shows the characteristics with pneumatic turbulators at 65% chord and an air volume flow of 80  $cm^3/sec$ . At the lower end of the low drag bucket for  $Re = 3 \times 10^6$ , where the laminar separation bubble in the case of not blowing is very small or absent, the pneumatic turbulators do not have any effect. In the remaining situations, up to  $C_l \approx 1.3$ , the drag decrease is dramatic. The effect on lift is negligible.

In Fig. 18, the measured characteristics of the new and the original airfoil are compared in practical conditions. While the drag of the new airfoil is slightly higher at  $C_l \approx 1.25$  (i.e., insignificant in terms of sailplane drag), the drag decreases to over 10% at low lift coefficients, and the maximum lift coefficient is slightly increased. Thus, though the calculated drag (Fig. 15) is lower than the measured drag, the predicted trends are in fair agreement with the measurements.

Also shown in Fig. 18 are the results where the air volume flow was obtained by means of an open-ended, forward-facing tube (diameter 4 mm) mounted on the tunnel wall. The same results, not shown here, were obtained with the air volume flow obtained from 80 orifices (diameter 0.6 mm, equally spaced at 8 mm) drilled at 90% chord of the lower surface, being the location with the highest pressure in the turbulent part of the airfoil.

Finally, Fig. 19 shows the results with the simulated bug pattern mentioned before.

The maximum lift coefficient is practically maintained (as intended) and the drag at positive angles of attack is lower than for the original airfoil (Fig. 10). However, even when the drag increase due to real insects should be half of the drag increase due to simulated insects at  $\alpha < 0^\circ$ , the pilot should (as always) be aware of the consequences of flying too fast with

contaminated leading edges.

Next, the tip airfoil was designed. The considerations were similar to the previous case with the addition of the severe limitation that the shape of the aileron should not alter. Several attempts resulted in a modification of mainly the lower surface (Fig. 23), thus making the outer wing suitable for the application of pneumatic turbulators. A comparison of potential flow pressure distributions and calculated characteristics is presented in Fig. 21 and 22. Again, the estimated effect of free flight conditions on the location of transition could be exploited. This airfoil was not tested in the wind tunnel.

Since the outer wing is formed by linear lofting, aileron deflections of plus and minus 5 degrees were examined at both the inner wing airfoil and the tip airfoil. No problems are expected, as far as the calculations are concerned.

#### SAILPLANE WING MODIFICATION AND FLIGHT PERFORMANCE TEST RESULTS

Experience gained with the weight penalty of the modification of the inner wing test segment indicated an increase in minimum wing loading of about 7%. For compensation, considering the climb performance of the unmodified sailplane, the inner wing airfoil was slightly more cambered, yielding a maximum lift coefficient of about 1.47. This airfoil, named DU 80-176V1, and the tip airfoil DU 80-141 were used in modifying the ASW-19B wing. Coordinates are given in Table 2 and 3.

After removing the white surface coat, the wing was modified by adding foam, a glass-fiber skin, light-weight filling material, respectively, and finally white surface paint. It was grinded down to the correct shape with the help of 15 templates (for each 0.5 m span position) and 8 additional nose templates.

Some 870 little tubes (pneumatic turbulators), weighing only 70 grams in total, were installed. As in the wind tunnel tests, the air volume flow needed for the pneumatic turbulators was obtained by pressurizing each wing half by means of a nozzle mounted on the

streamline cap which covered the aileron actuator. Flight experiments showed that a nozzle diameter of only 6.5 mm was needed to obtain the right internal wing pressure.

Fig. 23 shows the performance curves of the sailplane before and after the wing modification, as measured by DFVLR, Institut für Flugmechanik, Braunschweig. At the moment of writing this paper, a detailed analysis of the new performance polar, using the computer program described in Ref. 11, has not yet been performed. However, the improvement is satisfying and beyond our expectations. Not shown is the performance curve obtained with the pneumatic turbulators inactive (covered by tape); the curve coincides with the polar of the unmodified sailplane. Obviously, the drag increase due to the pronounced laminar separation bubbles on the lower surface with inactive turbulators, is equal to the sum of the drag reductions of the improved upper and lower surface with active turbulators.

Stalling behaviour is very gentle, and a test with the wing surface entirely wetted in flight by water drained from the DFVLR test sailplane, a Cirrus, revealed no change in minimum flight speed in comparison to the clean wing case.

#### ACKNOWLEDGEMENT

The authors are indebted to their colleagues at the Low Speed Laboratory for their pleasant and valuable support, to Mr. M. Wijnheijmer for performing the wind tunnel tests on the outer wing segment, to Mr. J. Nieuwland and Mr. M. Jutte for manufacturing the templates, to the Dutch crew which assisted in modifying the wing, to the colleagues at DFVLR Braunschweig for their pleasant cooperation and careful flight performance measurements and, last but not least, to the manufacturer of the ASW-19B, Alexander Schleicher Segelflugzeugbau, and the designer, Mr. G. Waibel, for their most appreciated support and interest.

## REFERENCES

1. Boermans, L.M.M., Selen, H.J.W., and Wijnheijmer, M.L., "Wind Tunnel Tests on Two Wing Segments of the ASW-19 Sailplane," Memorandum M-379, Delft University of Technology, Dept. Aerospace Engineering, August 1980.
2. Van Ingen, J.L., Boermans, L.M.M., and Blom, J.J.H., "Low Speed Airfoil Section Research at Delft University of Technology," ICAS-80-10.1, October 1980.
3. Althaus, D., "Stuttgarter Profilkatalog I," Institut für Aero- und Gasdynamik der Universität Stuttgart, 1972.
4. Gooden, J.H.M., "Experimental Low Speed Aerodynamic Characteristics of the Wortmann FX 66-S-196V1 Airfoil," OSTIV - Publication XV.
5. Zacher, H., "Messungen zum Einfluss der Insektenrauhigkeit auf die Flugleistungen," Aerokurier 2, 1978.
6. Coleman, W.S., "Roughness due to Insects," Boundary Layer and Flow Control, Volume 2, G.V. Lachmann, Ed., Pergamon Press, pp. 682-747, 1961.
7. Johnson, R.H., "A Flight Test Evaluation of the Standard Cirrus B," Soaring, March 1976.
8. Horstmann, K.H. and Quast, A., "Drag Reduction by Pneumatic Turbulators," OSTIV Congress, Paderborn, West Germany, 1981.
9. Wortmann, F.X., "Progress in the Design of Low Drag Airfoils," Boundary Layer and Flow Control, Vol. 2, G.V. Lachmann, Ed., Pergamon Press, pp. 748-770, 1961.
10. Pfenninger, W., "Untersuchungen über Reibungsverminderungen an Tragflügeln, Insbesondere mit Hilfe von Grenzschichtabsaugung," Mitteilung 13 der ETH, Zurich, 1946.
11. Boenmans, L.M.M., "Development of a Computer Program for Parametric Sailplane Performance Optimization," OSTIV Publication XV.
12. Head, M.R., "Transition due to Roughness," J.R. Aeron. Soc. Vol. 69, pp. 344-345, 1965.

## APPENDIX

In Coleman's comprehensive work with respect to the insect problem (Ref. 6), it is shown that in most practical cases

- certainly in the present ones - the differential equations which rule the insect trajectory may be solved by assuming that the parameter

$$\mathcal{K} = \frac{1}{2} \cdot c_d \cdot \frac{c}{l} \cdot \frac{\rho_{air}}{\rho_{insect}}$$

is a constant. This parameter links the size, density and drag coefficient of the insect with the size of the airfoil and density of the air. As a result, the trajectory of an insect is independent of the velocity of the approaching airfoil, and impact velocities can be presented in dimensionless form against the fractional chord position, similar to the velocity distribution of an airfoil set at a particular angle of attack.

When the component of the impact velocity normal to the surface is greater than a particular value, termed rupture velocity, the insect will disintegrate and stick to the surface or leave a trace. This rupture velocity varies between species.

Coleman measured, in a wind tunnel, rupture velocities of 10<sup>m</sup>/s (Aphid), 12<sup>m</sup>/s (house fly), 14<sup>m</sup>/s (fruit fly *Drosophila*) and 20<sup>m</sup>/s (*Mormoniella*, a pupal parasite of the house fly about the same size as an Aphid). Field experiments showed a mean value of 11<sup>m</sup>/s with possible variations of 1.8<sup>m</sup>/s. Since the extent of the impacts depends on the most fragile insects encountered, the Aphid is most suitable for such experiments.

From these considerations, interesting conclusions can be drawn that for a particular airfoil and aerial insect population, the roughness height distribution of the remains and the extent of the insect impacts, in terms of fractional chord, depends on speed and angle of attack, not on the size of the airfoil. The number of impacts is related to the size of the airfoil. Moreover, in Ref. 12 it is shown that when the size of an airfoil is increased from chord length  $c_1$  to  $c_2$  and the speed (exactly: the unit Reynolds number  $u/v$ ) remains unchanged, the tolerable roughness height increases as  $c_2^{1/4}/c_1$ . Thus, doubling the size of an airfoil means an increase in tolerable roughness height of only 19%.

Combining the foregoing arguments leads to some practical conclusions:  
 - Two wings with similar shape but different size, flying at equal wing loading, are equally sensitive to insect contamination. However, the bigger one may have a higher drag coefficient because of the greater number of insects it captures.

- The taper ratio of a wing with continuous airfoil shape does not influence the local sensitivity of the flow for insect contamination. However, the number of insects, and in consequence the local drag coefficient, may increase towards the wing root.

		NO FLAP				FLAP		
Type		ASW-19B	St. Cirrus	Astir	KA-6CR	Nimbus II	LS-3A	Vega
Wing loading	kgf/m <sup>2</sup>	31.7	29	29	22.6	30.6	31.6	31.4
Airfoil		FX61-163	(*)	E 603	NACA 63 <sub>2</sub> -618-K4	FX67-K-170	FX67-K-170	FX67-K-150
Distance from wing root	m.	1.50	1.50	1.50	3.25	2.65	1.50	1.50
Local chord	m.	0.83	0.81	0.95	0.87	0.84	0.83	0.79
Local thickness	%C	16.3	19.2	19.2	15.8	17.0	17.0	15.0
Flight time	min.	187	230	223	267	195	282	190
Starts		2	1	1	3	1	3	1
Impacts	Total	457	420	455	247	466	613	283
Distribution in	upper	48	56	58	55	84	75	75
% of total	lower	52	44	42	45	16	25	25
Extend in	upper	12	18	16	7	20	19	15
% chord	lower	14	15	16	9	4	5	5
Impacts 1%C	% total	33	38	37	57	34	35	41
Distribution in	upper	19	23	22	28	24	24	28
% of total	lower	14	15	15	29	10	12	13
Impacts 2%C	% total	57	54	55	81	53	54	64
Distribution in	upper	31	32	32	39	38	36	45
% of total	lower	26	22	23	42	15	18	19

(\*) FX66S02-196 → FX66-17AII-182

Table 1: Results of insect impact measurements on two sheets of self-adhesive matted polyester film (0.59 m. wide), attached to the left and right wing at equal distance from the wing root.

DU 80-141

Nr	X (%)	Y (%)	X (%)	Y (%)	Nr	X (%)	Y (%)
0001	100.00000	0.00000	100.00000	0.00000	0052	.25549	.97386
0002	99.88174	.06243	99.88174	.06243	0053	.04938	.39796
0003	99.54541	.23599	99.54541	.23599	0054	0.00000	0.00000
0004	99.04251	.47424	99.04251	.47424	0055	.00616	-.12823
0005	98.38052	.75230	98.38052	.75230	0056	.14861	-.59999
0006	97.55237	1.03567	97.55237	1.03567	0057	.49384	-1.01460
0007	96.53253	1.31286	96.53253	1.31286	0058	1.05573	-1.30895
0008	95.31020	1.60188	95.31020	1.60188	0059	1.82674	-1.74793
0009	93.89580	1.91302	93.89580	1.91302	0060	2.79160	-2.09413
0010	92.30186	2.24424	92.30186	2.24424	0061	3.93886	-2.42052
0011	90.53435	2.59089	90.53435	2.59089	0062	5.26358	-2.72275
0012	88.59871	2.95497	88.59871	2.95497	0063	6.76016	-2.99330
0013	86.50539	3.33893	86.50539	3.33893	0064	8.42525	-3.24474
0014	84.26730	3.74219	84.26730	3.74219	0065	10.25488	-3.46755
0015	81.88638	4.16230	81.88638	4.16230	0066	12.24149	-3.65754
0016	79.40652	4.59872	79.40652	4.59872	0067	14.37355	-3.83038
0017	76.81168	5.04628	76.81168	5.04628	0068	16.64122	-3.98454
0018	74.12476	5.50151	74.12476	5.50151	0069	19.03639	-4.10000
0019	71.35989	5.96067	71.35989	5.96067	0070	21.54681	-4.19080
0020	68.33644	6.41261	68.33644	6.41261	0071	24.16104	-4.26213
0021	65.45068	6.86972	65.45068	6.86972	0072	26.86833	-4.30453
0022	62.52605	7.31061	62.52605	7.31061	0073	29.65771	-4.30999
0023	59.57496	7.83031	59.57496	7.83031	0074	32.51628	-4.28441
0024	56.61040	8.22207	56.61040	8.22207	0075	35.43161	-4.23257
0025	53.64100	8.57968	53.64100	8.57968	0076	38.39252	-4.13381
0026	50.67599	8.89989	50.67599	8.89989	0077	41.38803	-4.00132
0027	47.72822	9.17641	47.72822	9.17641	0078	44.40536	-3.82510
0028	44.80505	9.40185	44.80505	9.40185	0079	47.43119	-3.60177
0029	41.90974	9.57577	41.90974	9.57577	0080	50.45075	-3.32581
0030	39.05399	9.69819	39.05399	9.69819	0081	53.45511	-2.96605
0031	36.24724	9.76544	36.24724	9.76544	0082	56.47122	-2.49767
0032	33.49496	9.77520	33.49496	9.77520	0083	59.53753	-1.93970
0033	30.80359	9.72879	30.80359	9.72879	0084	62.67820	-1.31371
0034	28.18259	9.62667	28.18259	9.62667	0085	65.90935	-.68546
0035	25.63982	9.47040	25.63982	9.47040	0086	69.27020	.11000
0036	23.18082	9.26256	23.18082	9.26256	0087	73.14774	.46792
0037	20.81703	9.00111	20.81703	9.00111	0088	76.25433	.67589
0038	18.55211	8.68723	18.55211	8.68723	0089	79.25183	.81535
0039	16.39134	8.32690	16.39134	8.32690	0090	82.11273	.89904
0040	14.34323	7.92229	14.34323	7.92229	0091	84.82059	.92901
0041	12.41335	7.47584	12.41335	7.47584	0092	87.35478	.90559
0042	10.60933	6.99164	10.60933	6.99164	0093	89.69197	.83331
0043	8.93680	6.47073	8.93680	6.47073	0094	91.80971	.72212
0044	7.39690	5.91553	7.39690	5.91553	0095	93.69296	.58908
0045	5.99348	5.33302	5.99348	5.33302	0096	95.32809	.44653
0046	4.73062	4.72792	4.73062	4.72792	0097	96.71445	.31980
0047	3.61137	4.10485	3.61137	4.10485	0098	97.86314	.21518
0048	2.63940	3.46983	2.63940	3.46983	0099	98.77252	.12636
0049	1.81383	2.82832	1.81383	2.82832	0100	99.43652	.05854
0050	1.13489	2.19431	1.13489	2.19431	0101	99.85661	.01526
0051	.61348	1.57749	.61348	1.57749	0102	100.00000	0.00000

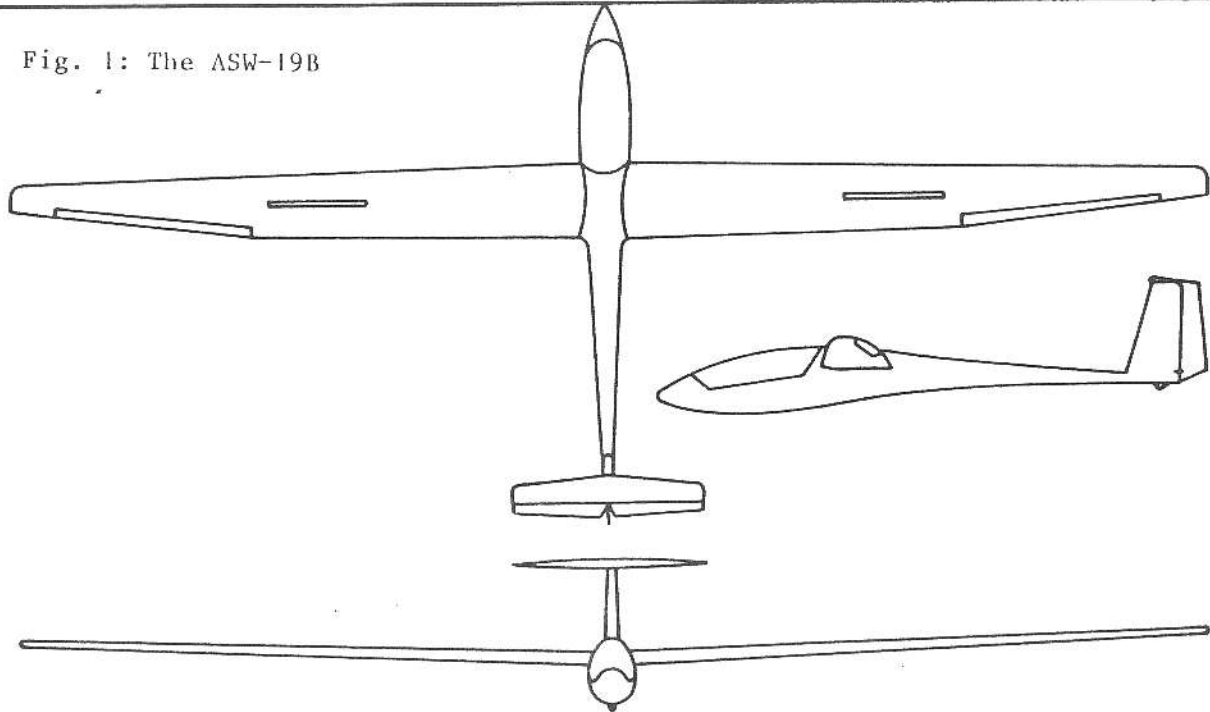
Table 3: Coordinates of DU 80-141

DU 80-176 V1

Nr	X (%)	Y (%)	X (%)	Y (%)	Nr	X (%)	Y (%)
0001	100.00000	0.00000	100.00000	0.00000	0052	.30264	1.03539
0002	99.87671	.06498	99.87671	.06498	0053	.06613	.43899
0003	99.52824	.24805	99.52824	.24805	0054	.00375	-.09381
0004	99.01393	.49313	99.01393	.49313	0055	.14961	-.55669
0005	98.31784	.75959	98.31784	.75959	0056	.53630	-.96297
0006	97.41879	1.03951	97.41879	1.03951	0057	1.15941	-1.35253
0007	96.30762	1.34046	96.30762	1.34046	0058	1.99156	-1.74560
0008	94.98752	1.67129	94.98752	1.67129	0059	3.02147	-2.12964
0009	93.46709	2.03633	93.46709	2.03633	0060	4.24290	-2.49943
0010	91.75551	2.43810	91.75551	2.43810	0061	5.64893	-2.85590
0011	89.86403	2.88048	89.86403	2.88048	0062	7.23210	-3.19906
0012	87.80823	3.36579	87.80823	3.36579	0063	8.98320	-3.52847
0013	85.60500	3.89185	85.60500	3.89185	0064	10.89279	-3.84181
0014	83.26942	4.45434	83.26942	4.45434	0065	12.95241	-4.13716
0015	80.81693	5.05042	80.81693	5.05042	0066	15.15269	-4.41358
0016	78.26517	5.67612	78.26517	5.67612	0067	17.48395	-4.66916
0017	75.63252	6.32454	75.63252	6.32454	0068	19.93602	-4.90336
0018	72.93744	6.98705	72.93744	6.98705	0069	22.49658	-5.11511
0019	70.19826	7.65219	70.19826	7.65219	0070	25.15584	-5.29993
0020	67.43169	8.30464	67.43169	8.30464	0071	27.90378	-5.45986
0021	64.64906	8.92551	64.64906	8.92551	0072	30.72441	-5.59479
0022	61.85374	9.49716	61.85374	9.49716	0073	33.60654	-5.69677
0023	59.04517	10.00893	59.04517	10.00893	0074	36.54153	-5.76754
0024	56.22295	10.45737	56.22295	10.45737	0075	39.51392	-5.80844
0025	53.39121	10.84195	53.39121	10.84195	0076	42.50764	-5.81355
0026	50.55665	11.16220	50.55665	11.16220	0077	45.51764	-5.78129
0027	47.72693	11.41698	47.72693	11.41698	0078	48.52441	-5.70997
0028	44.90945	11.60515	44.90945	11.60515	0079	51.51664	-5.59553
0029	42.11204	11.72670	42.11204	11.72670	0080	54.48163	-5.43446
0030	39.34285	11.78120	39.34285	11.78120	0081	57.40424	-5.22252
0031	36.60884	11.76834	36.60884	11.76834	0082	60.26510	-4.94881
0032	33.91737	11.69060	33.91737	11.69060	0083	63.05347	-4.58236
0033	31.27759	11.55003	31.27759	11.55003	0084	65.79395	-4.08350
0034	28.69792	11.34723	28.69792	11.34723	0085	68.54282	-3.45241
0035	26.18600	11.08452	26.18600	11.08452	0086	71.34120	-2.74105
0036	23.75008	10.76425	23.75008	10.76425	0087	74.18854	-2.01017
0037	21.39771	10.38850	21.39771	10.38850	0088	77.06526	-1.30310
0038	19.13591	9.96000	19.13591	9.96000	0089	79.94682	-.66265
0039	16.97119	9.48191	16.97119	9.48191	0090	82.79379	-.12892
0040	14.90981	8.95874	14.90981	8.95874	0091	85.55432	.27363
0041	12.95879	8.39524	12.95879	8.39524	0092	88.17348	.53594
0042	11.12462	7.79504	11.12462	7.79504	0093	90.59715	.66432
0043	9.41261	7.16298	9.41261	7.16298	0094	92.78001	.68244
0044	7.82845	6.50465	7.82845	6.50465	0095	94.69386	.62176
0045	6.37755	5.82481	6.37755	5.82481	0096	96.32361	.50977
0046	5.06372	5.12871	5.06372	5.12871	0097	97.65866	.35928
0047	3.89038	4.42377	3.89038	4.42377	0098	98.69041	.22426
0048	2.86205	3.71780	2.86205	3.71780	0099	99.41933	.10247
0049	1.98338	3.01845	1.98338	3.01845	0100	99.85097	.02600
0050	1.26010	2.33545	1.26010	2.33545	0101	100.00000	0.00000
0051	.69930	1.67347	.69930	1.67347			

Table 2: Coordinates of DU 80-176 V1

Fig. 1: The ASW-19B


**ASW-19B**
**Wing**

span	15 m
area	11.0 m <sup>2</sup>
aspect ratio	20.45
airfoils	FX61-163 (inner wing) FX60-126 (tip)
root chord	0.91 m
tip chord	0.40 m
sweep (0.25 chord)	0°
twist	0° inner wing, -2° tip

**Fuselage**

length	6.80 m
breadth	0.63 m
depth	0.81 m

**Tail**

hor. tail area	1.10 m <sup>2</sup>
hor. tail airfoil	FX71-L-150/30 (12%)
vert. tail area	1.0 m <sup>2</sup>
vert. tail airfoil	FX71-L-150/30 (13.5%)

**Weight**

empty weight	245 kg
max. useful load	115 kg
max. water ballast	100 kg
all-up weight with ballast	454 kg
wing loading at 85 kg useful load	30 kg/m <sup>2</sup>
wing loading at permissible all-up weight	41.3 kg/m <sup>2</sup>

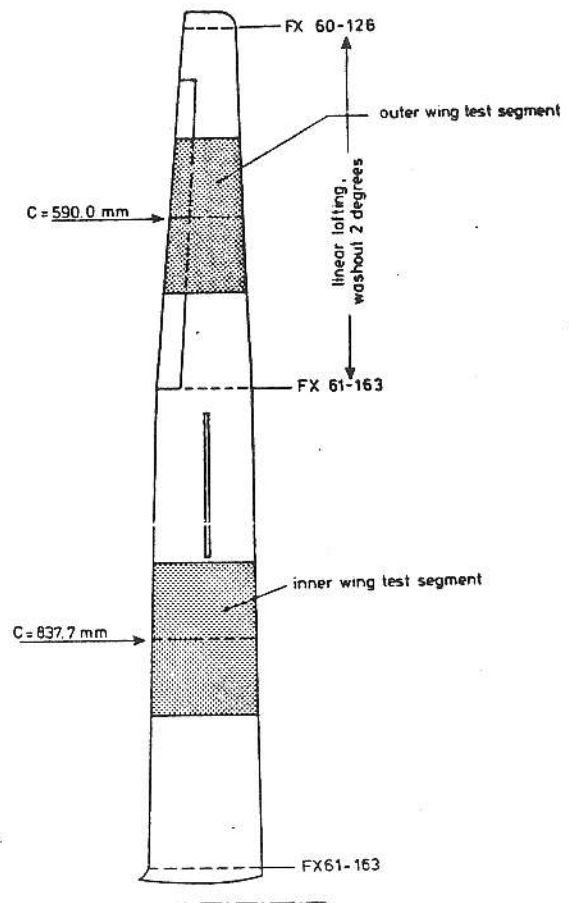


Fig. 2: Position of the test segments in the ASW-19B wing.

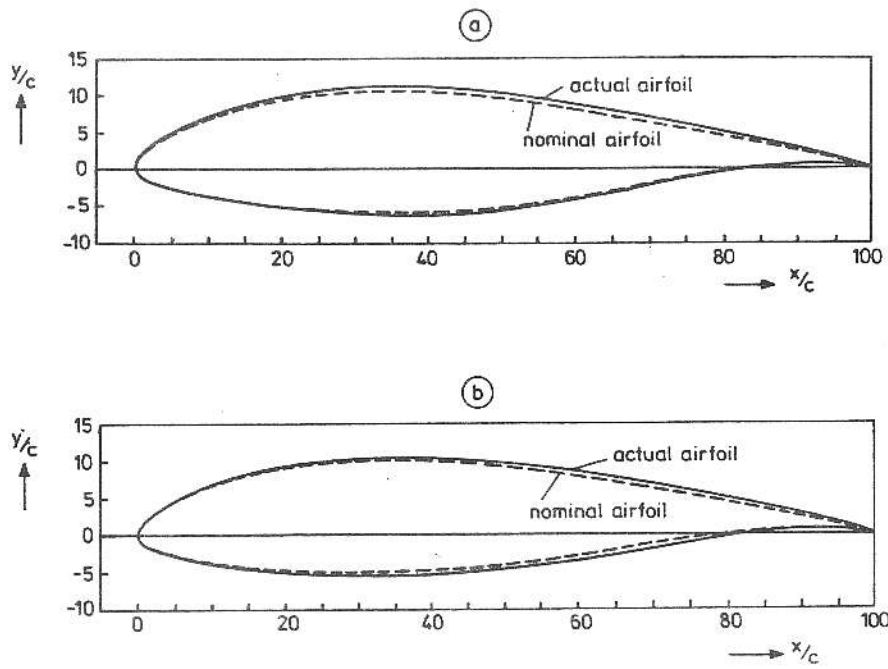


Fig. 3: Actual and nominal airfoil sections at the midspan position of (a) the inner wing test segment and (b) the outer wing test segment.

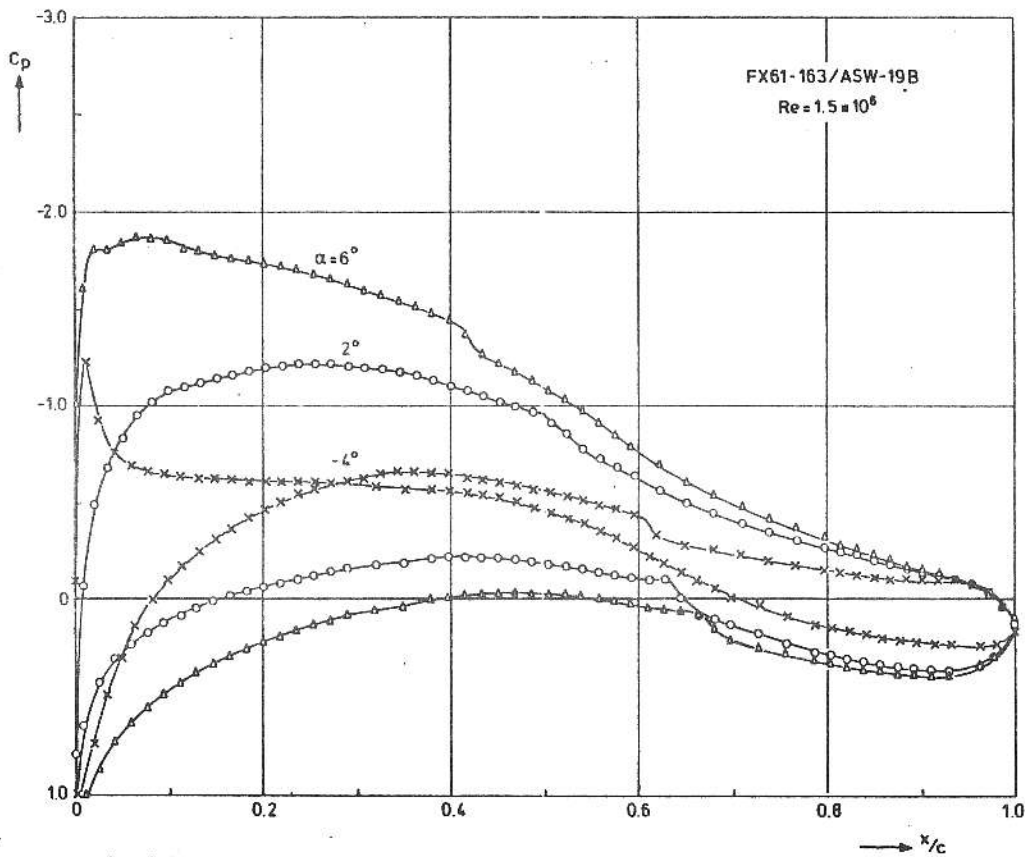


Fig. 4.1: Measured pressure distributions of the inner wing airfoil section.

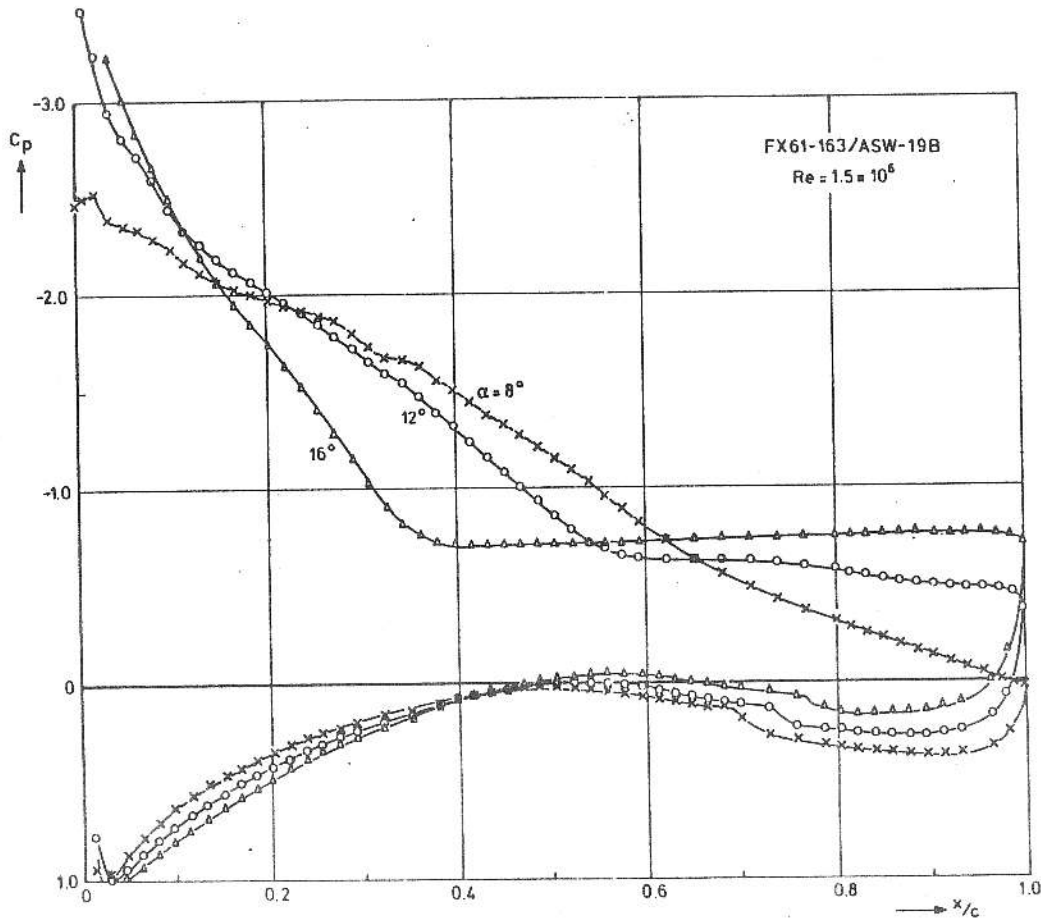


Fig. 4.2: Measured pressure distributions of the inner wing airfoil section.

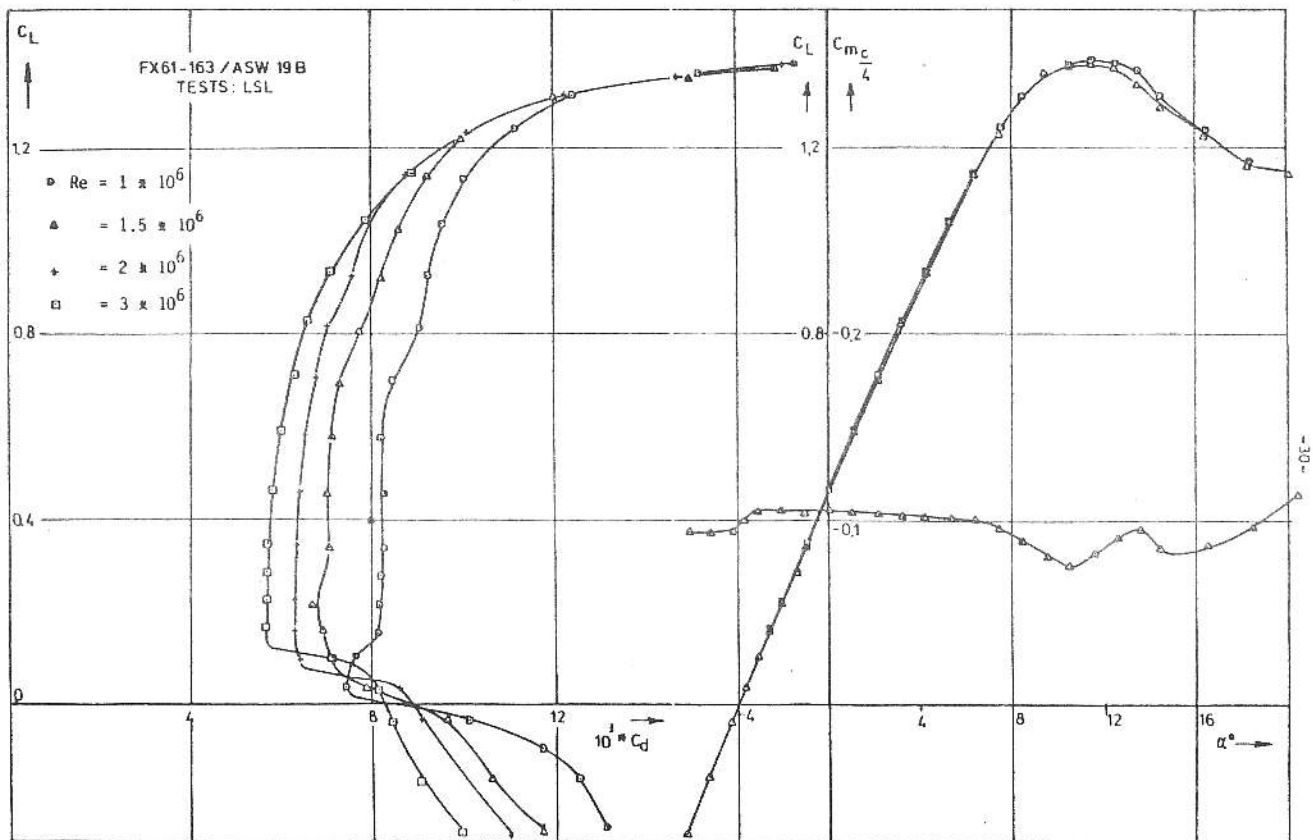


Fig. 5: Measured aerodynamic characteristics of the inner wing airfoil section.

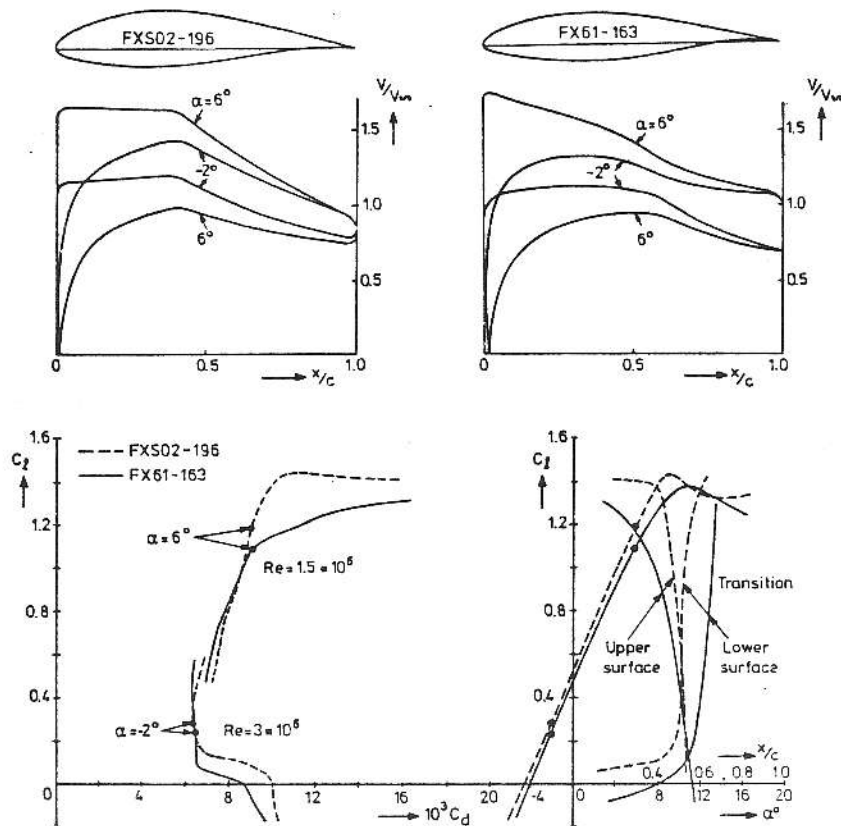
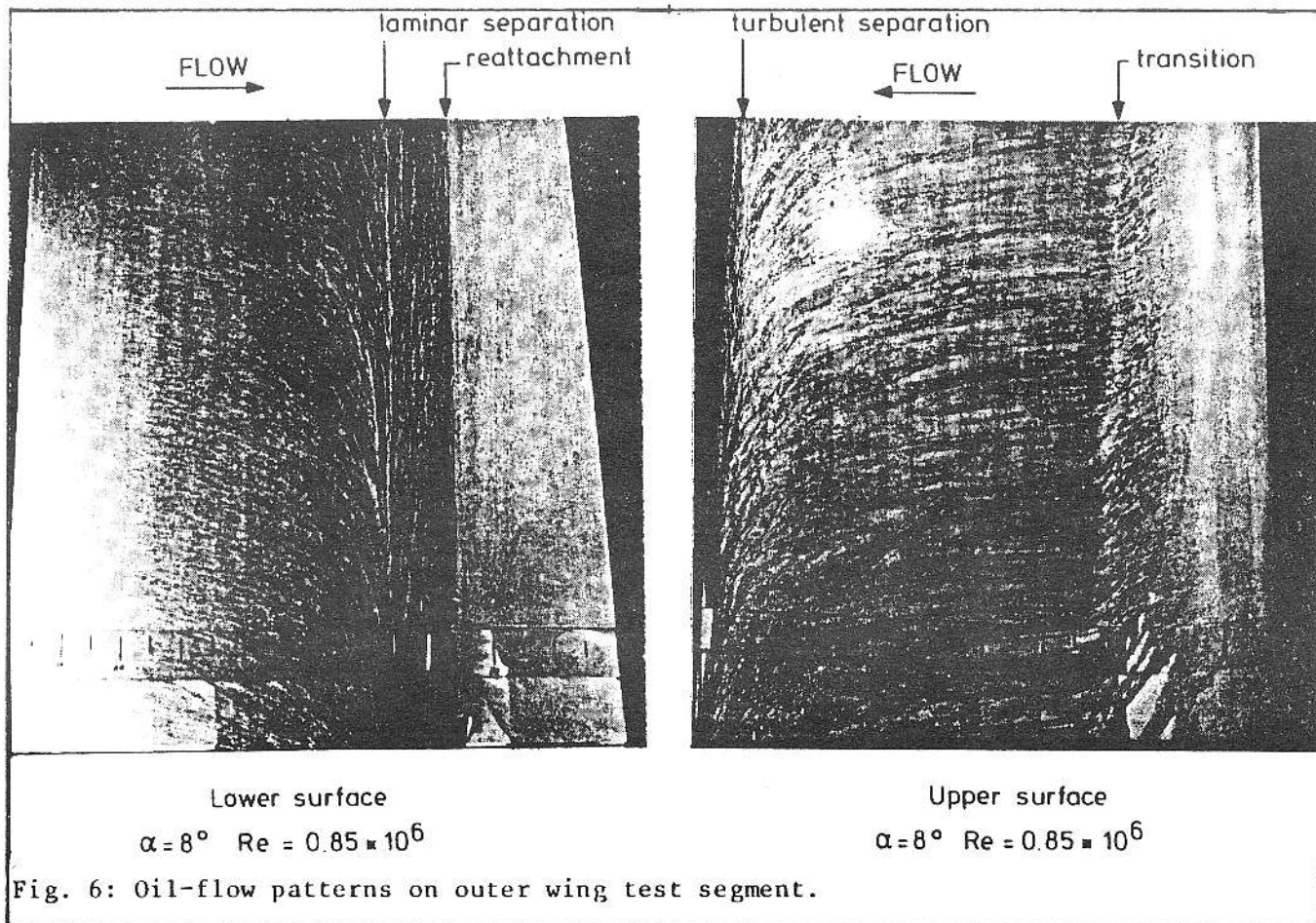


Fig. 7: Comparison of some typical airfoil characteristics. Measurements: Stuttgarter Laminarwindkanal, Ref. 3.

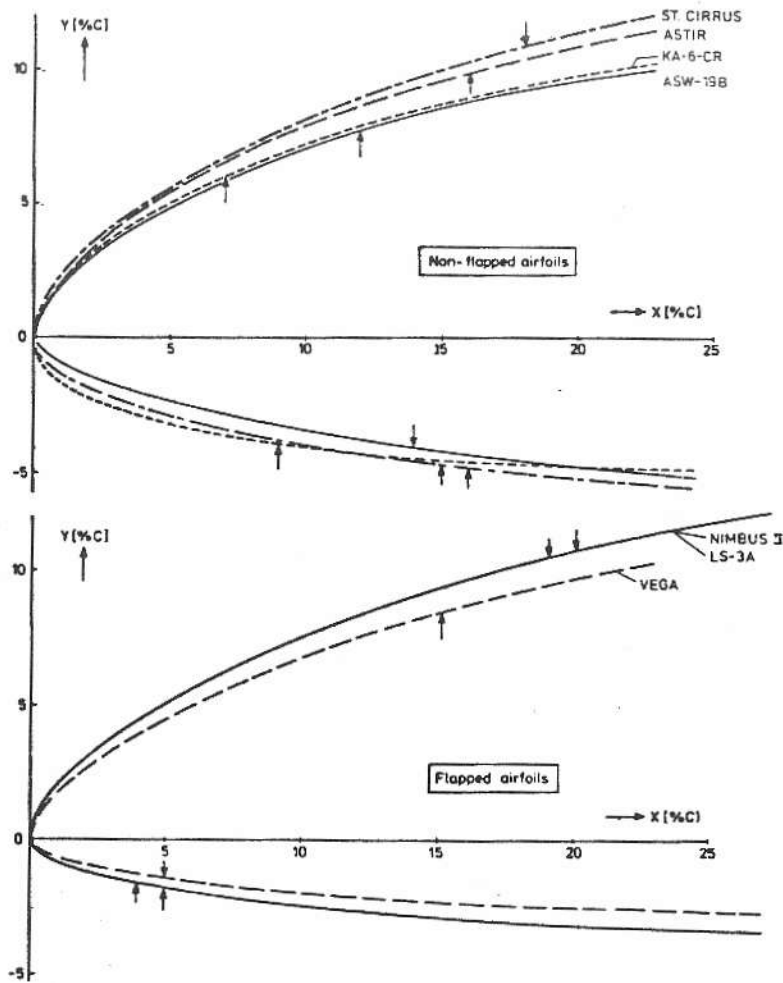


Fig. 8: Extent of insect impact pattern on some flapped and non-flapped airfoils.

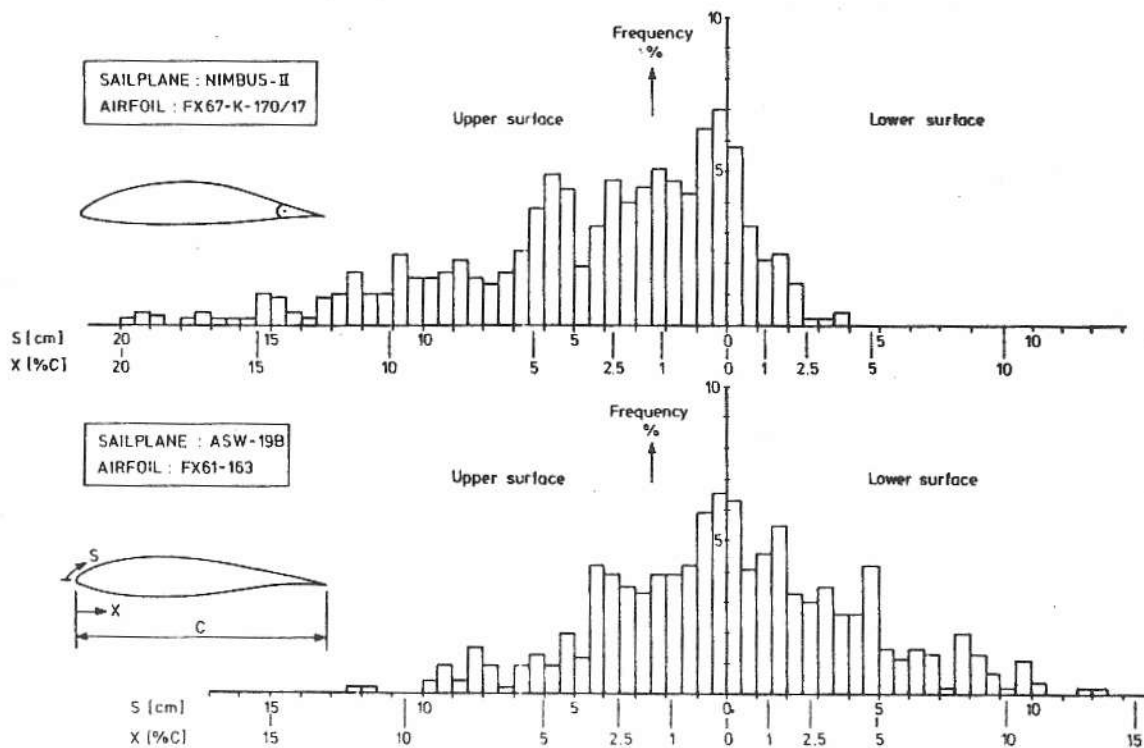


Fig. 9: Insect impact distribution on a flapped and a non-flapped airfoil.

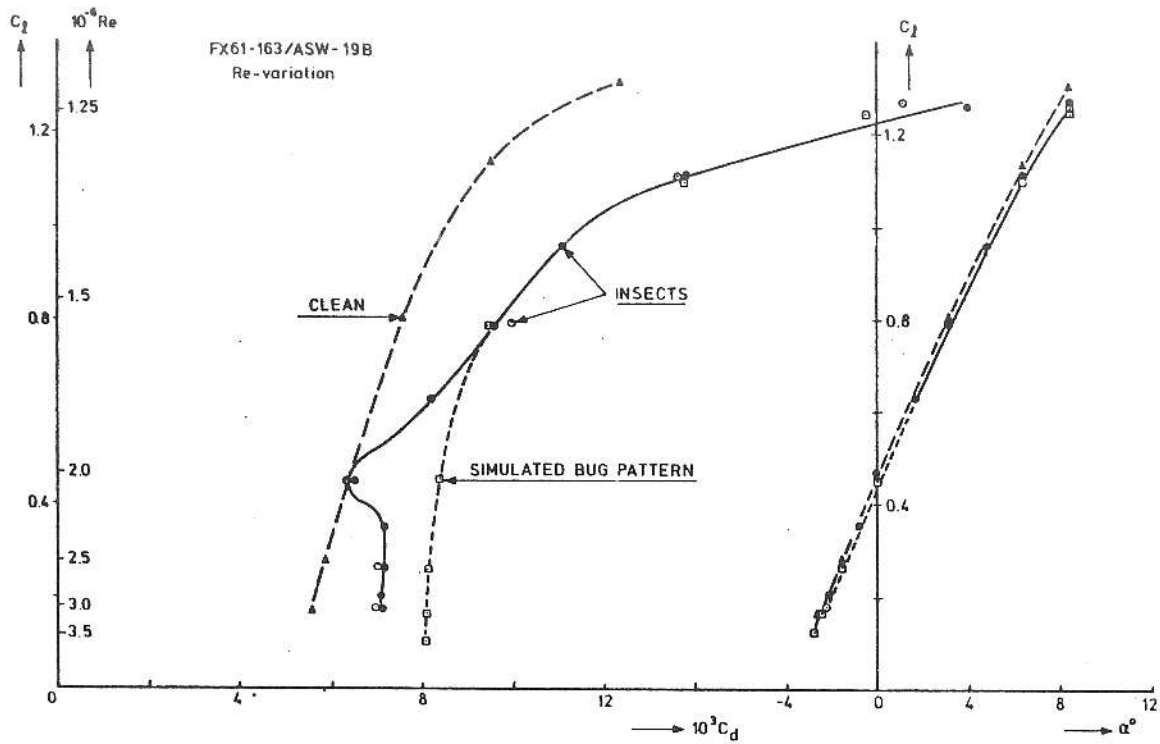


Fig. 10: Effect of the artificially and naturally roughened leading edge (two species) on the characteristics of the ASW-19B inner wing airfoil.

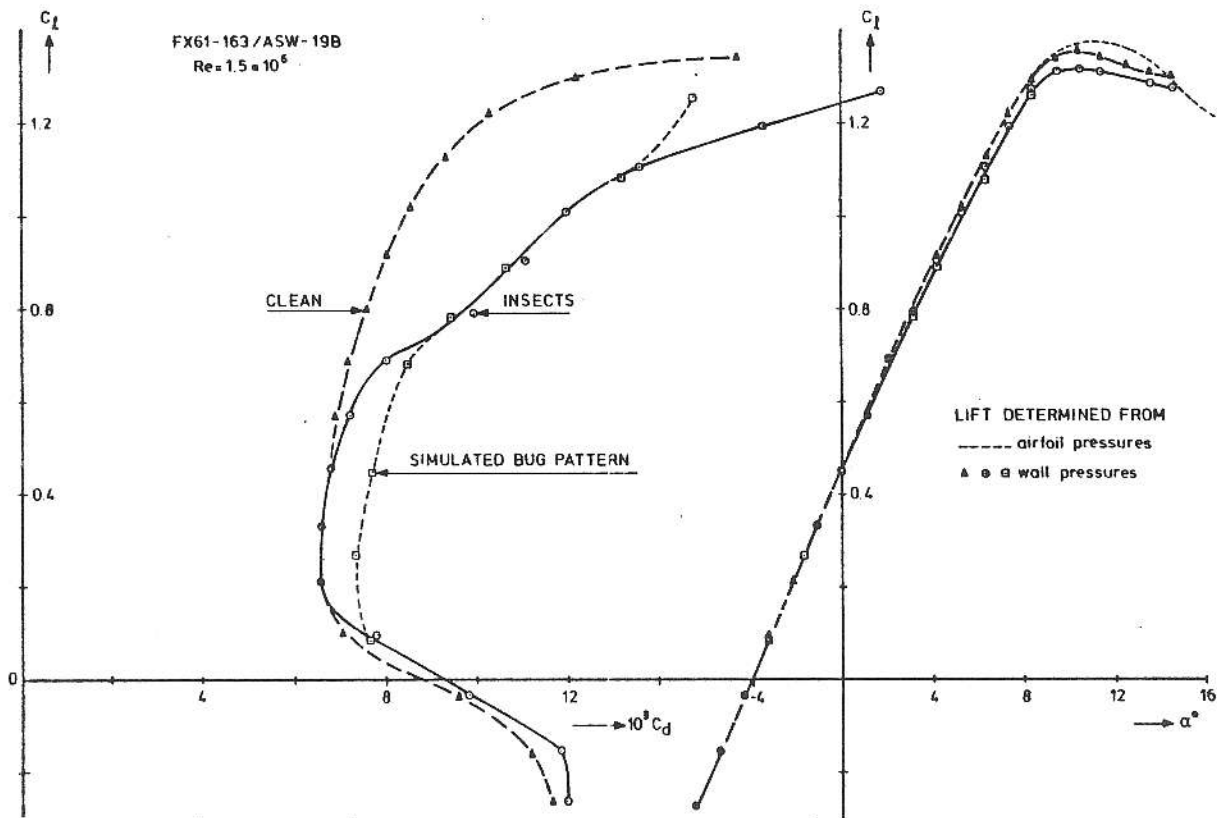


Fig. 11: Effect of the artificially and naturally roughened leading edge on the characteristics of the ASW-19B inner wing airfoil.  $Re = 1.5 \times 10^6$ .

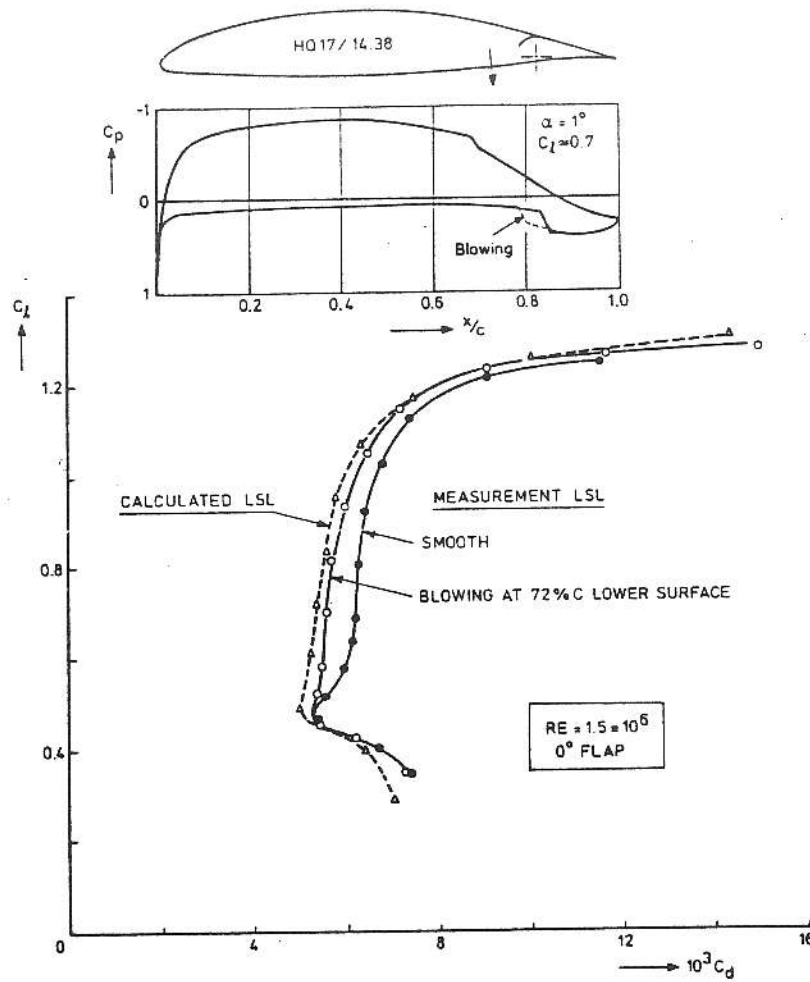


Fig. 12: Measured and calculated characteristics of HQ17/14.38.

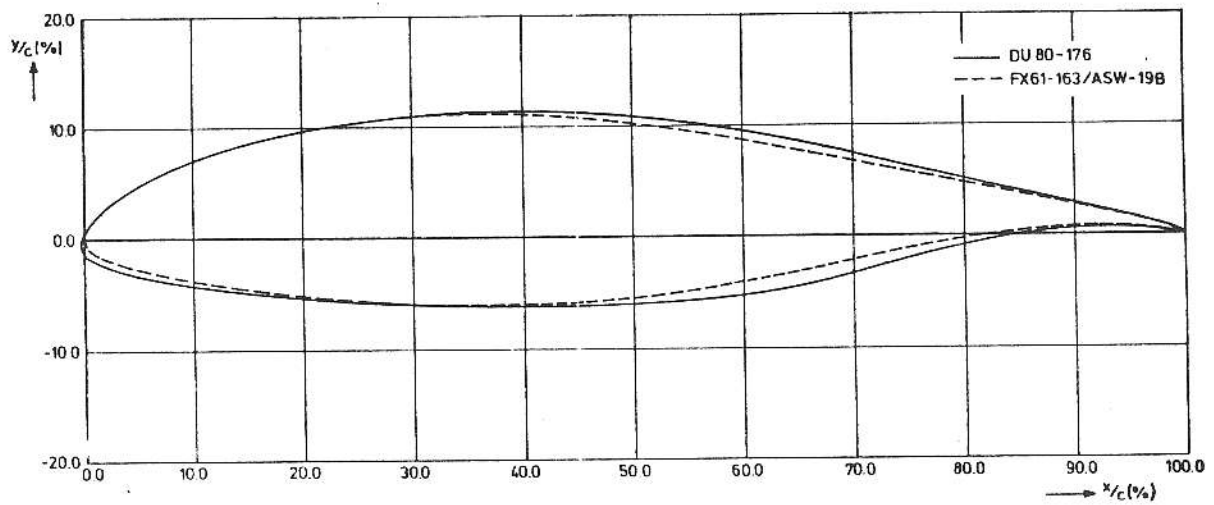


Fig. 13: The new airfoil fitted to the airfoil of the inner wing test segment.

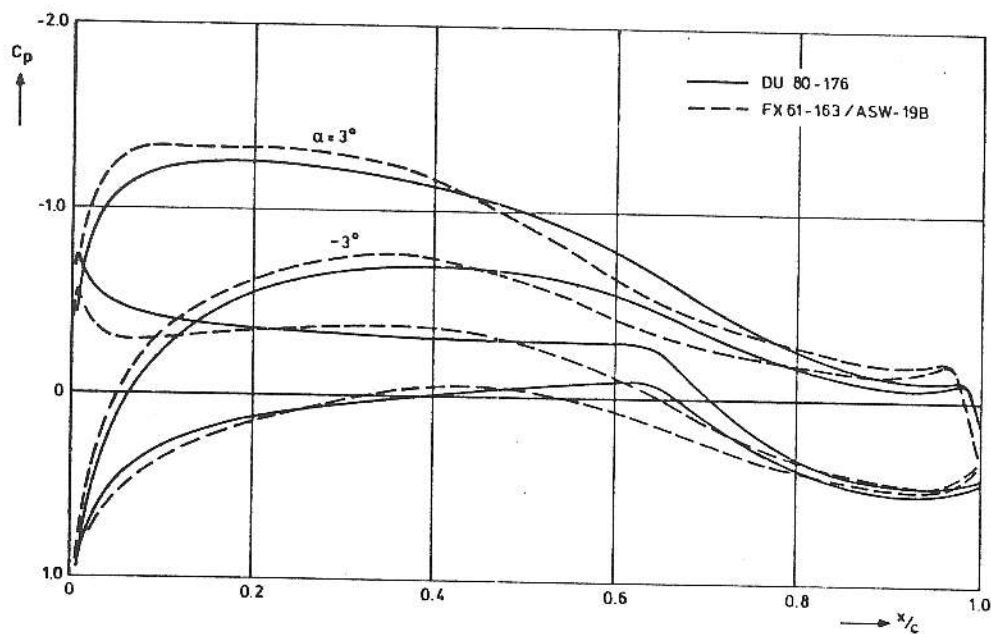


Fig. 14: Comparison of potential flow pressure distributions.

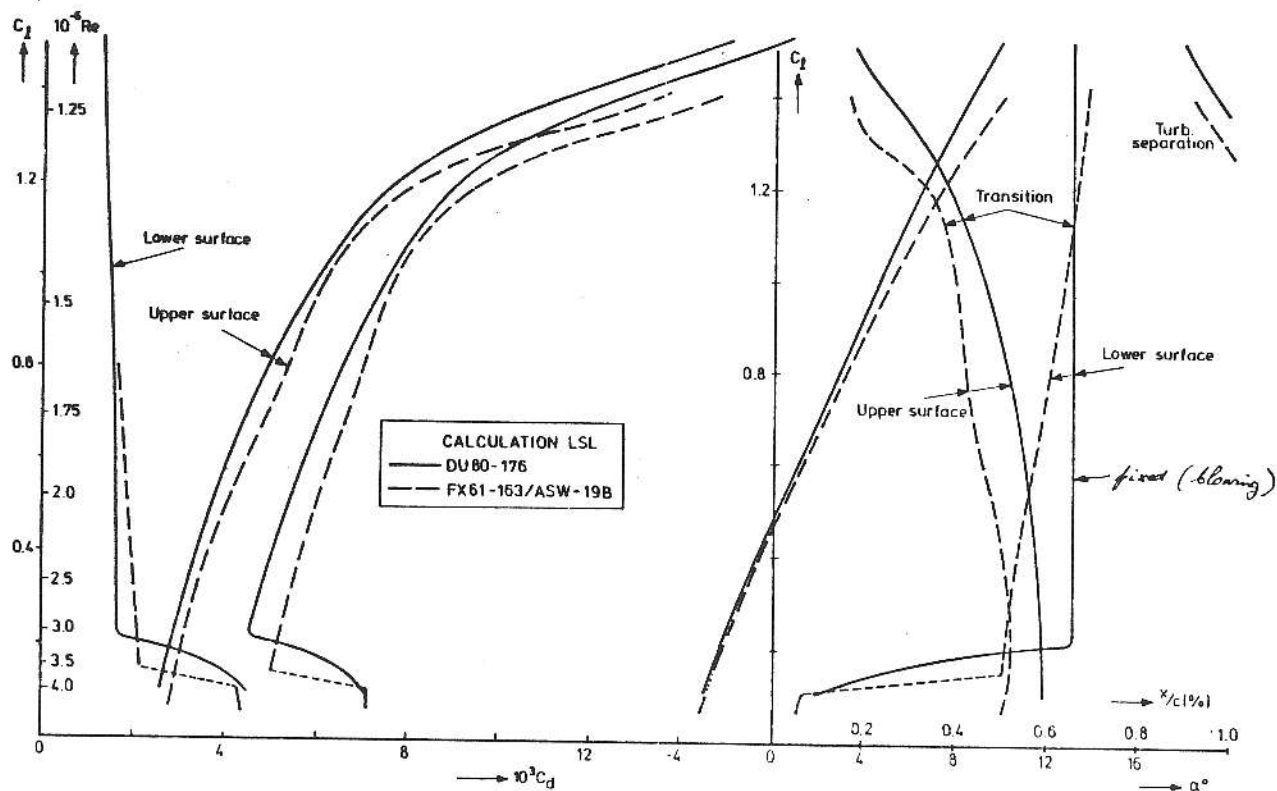


Fig. 15: Comparison of calculated characteristics.

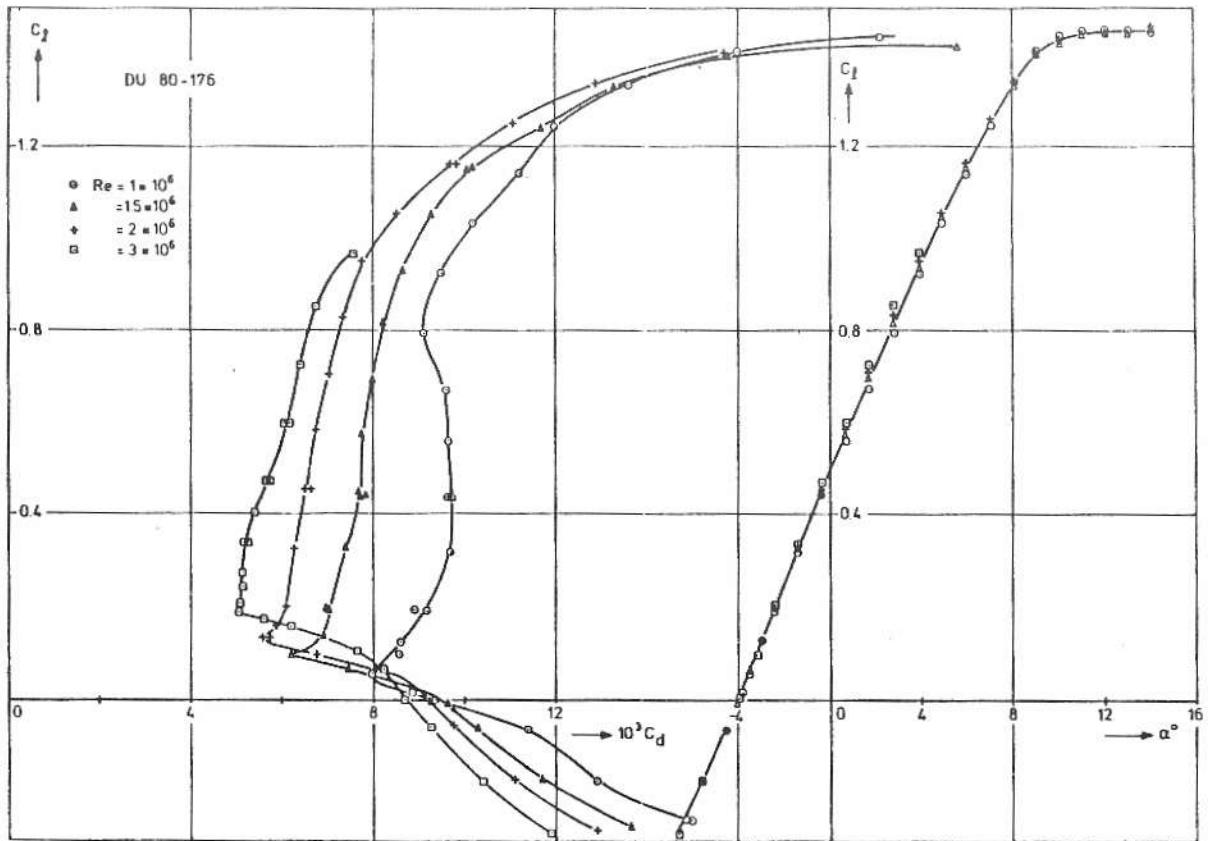


Fig. 16: Measured aerodynamic characteristics of DU80 176.

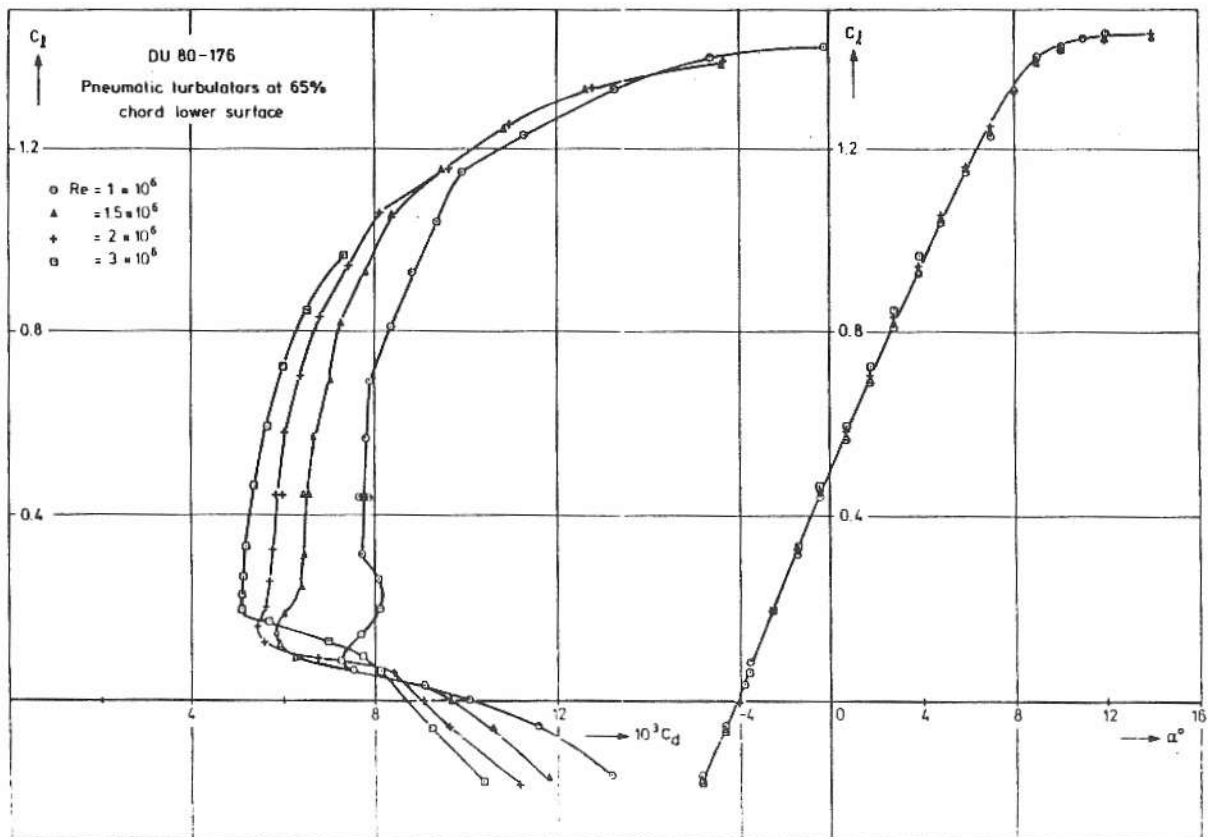


Fig. 17: Measured aerodynamic characteristics of DU80-176 with pneumatic turbulators.

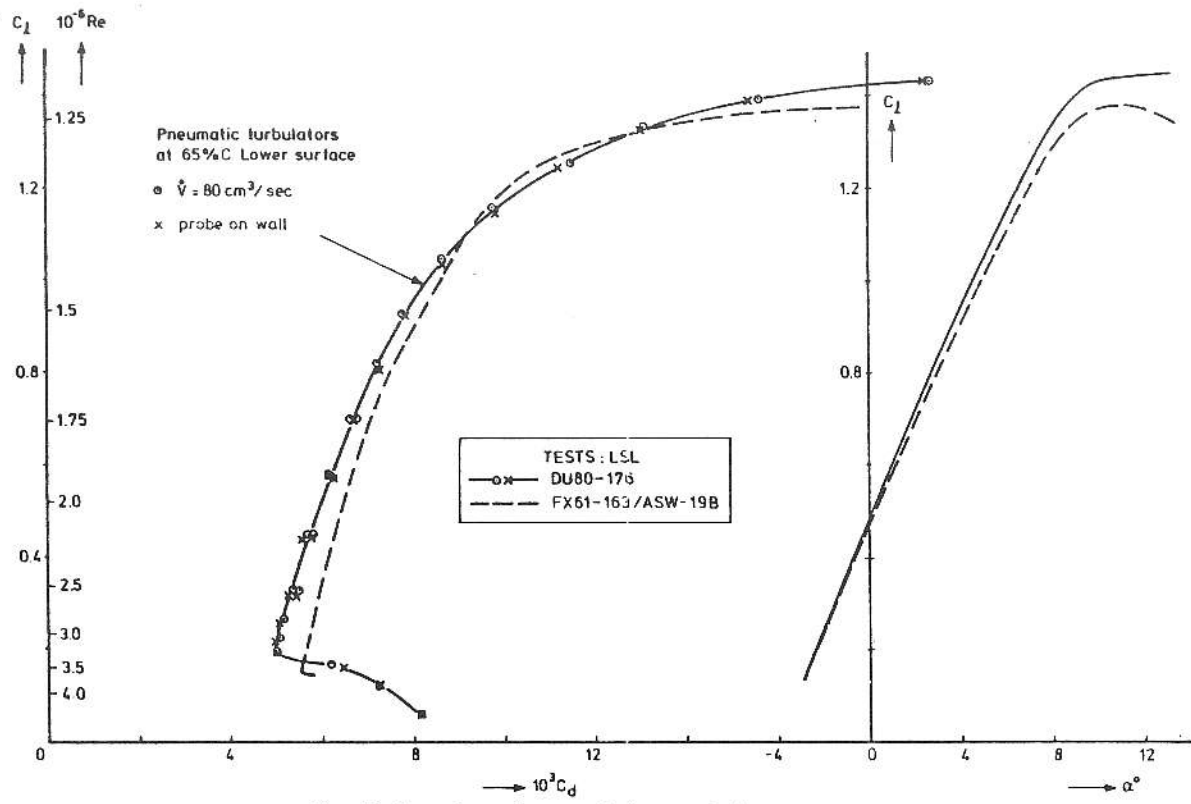


Fig. 18: Comparison of measured characteristics.

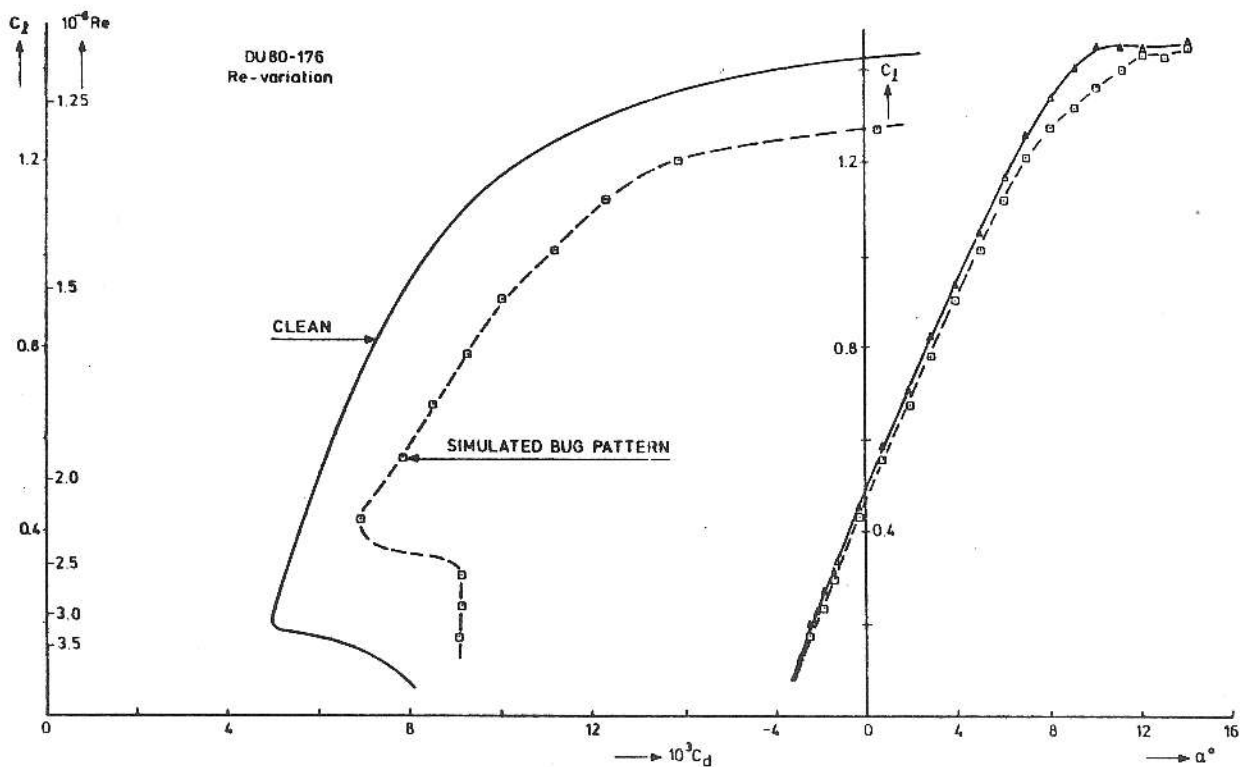


Fig. 19: Effect of the artificially roughened leading edge on the characteristics of airfoil DU80-176.

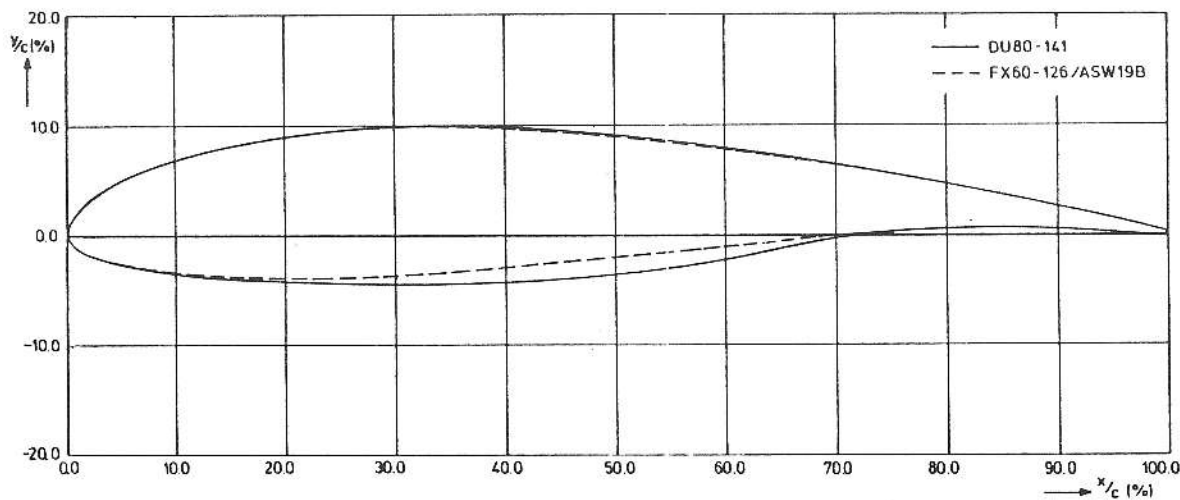


Fig. 20: The new tip airfoil fitted to the actual tip airfoil of the ASW-19B.

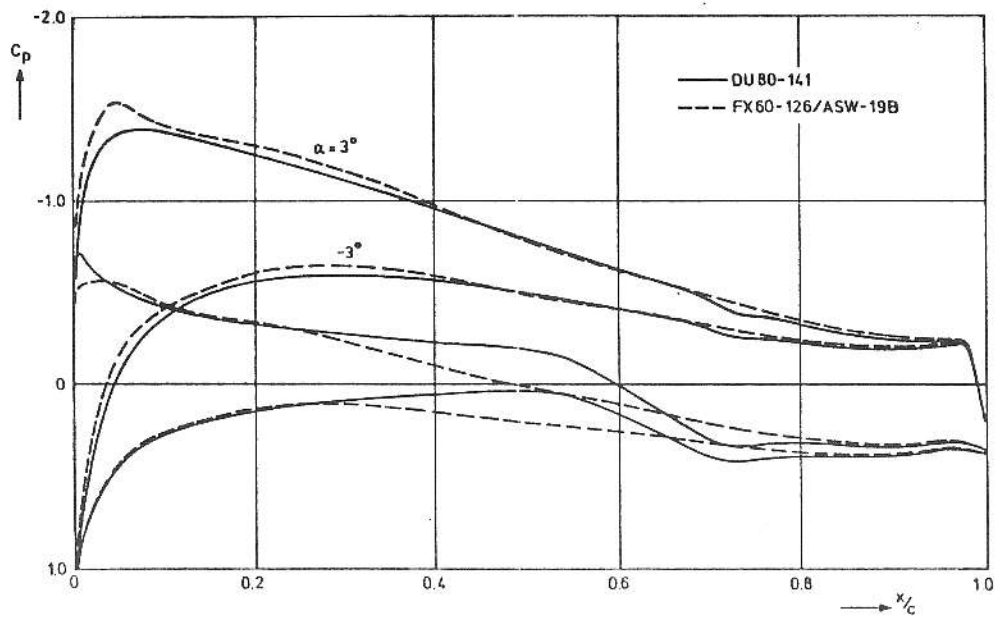


Fig. 21: Comparison of potential flow pressure distributions.

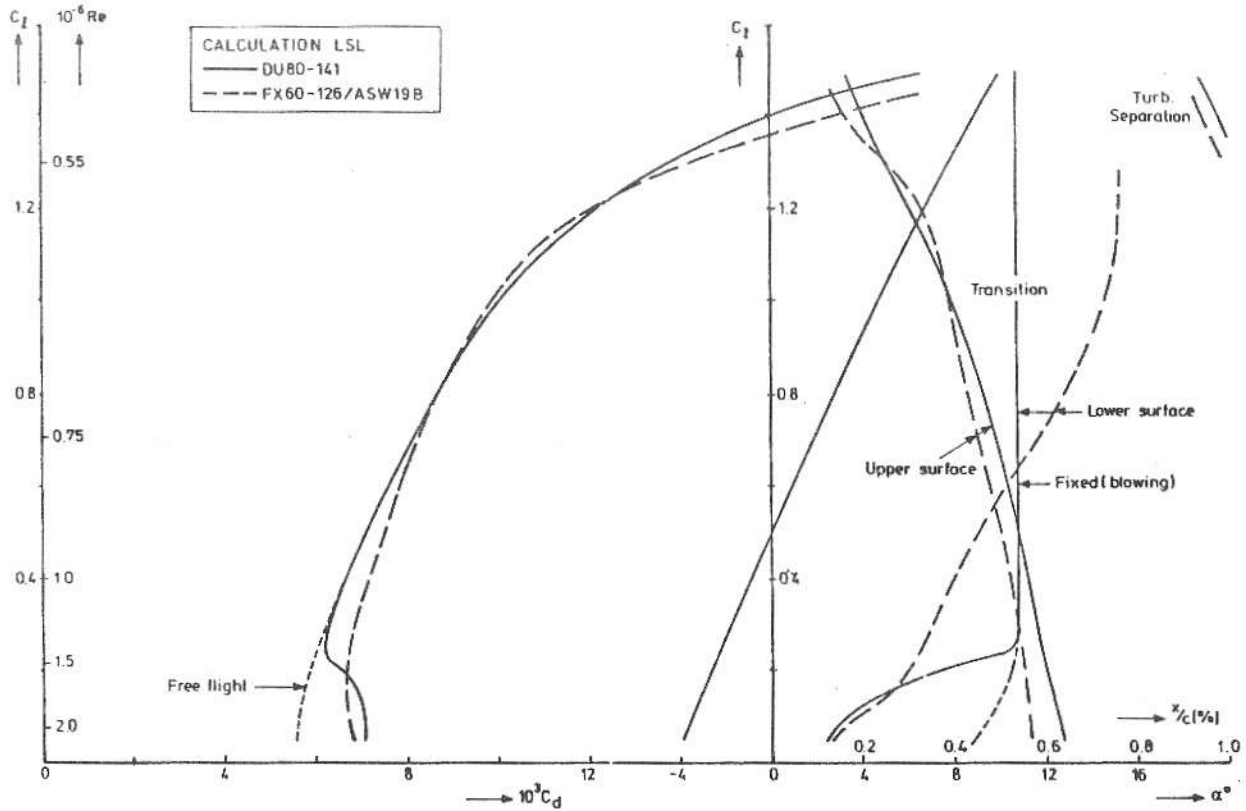


Fig. 22: Comparison of calculated characteristics for the tip airfoils.

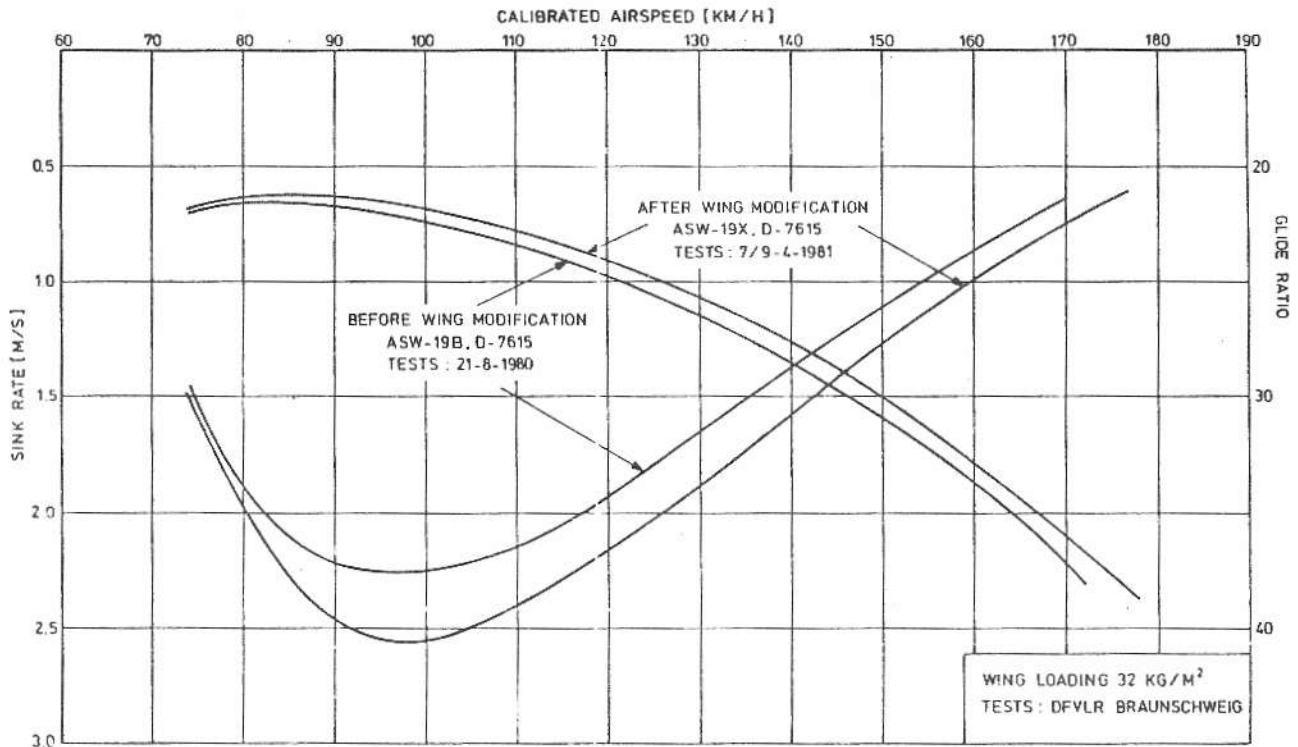


Fig. 23: Measured flight performance polars, before and after the wing modification.